IEEE Access
Multidisciplinary : Rapid Review : Open Access Journal

Received July 1, 2019, accepted July 17, 2019, date of publication July 22, 2019, date of current version August 7, 2019.

Digital Object Identifier 10.1109/ACCESS.2019.2930237

Robust Adaptive Neural-Network Backstepping Control Design for High-Speed Permanent-Magnet Synchronous Motor Drives: Theory and Experiments

FAYEZ F. M. EL-SOUSY[1,4], (Member, IEEE), MOHAMED F. EL-NAGGAR[1,2], MAHMOUD AMIN[3,4], (Senior Member, IEEE), AHMED ABU-SIADA[5], (Senior Member, IEEE), AND KHALED A. ABUHASEL[6]

[1]Electrical Engineering Department, College of Engineering, Prince Sattam Bin Abdulaziz University, Al-Kharj 11942, Saudi Arabia
[2]Faculty of Engineering, Electrical Engineering Department, Helwan University, Helwan 11795, Egypt
[3]Electrical and Computer Engineering Department, Manhattan College, New York, NY 10471, USA
[4]Department of Power Electronics and Energy Conversion, Electronics Research Institute, Giza 12622, Egypt
[5]Electrical and Computer Engineering Department, Curtin University, Perth, WA 6845, Australia
[6]Mechanical Engineering Department, College of Engineering, University of Bisha, Aseer 61421, Saudi Arabia

Corresponding author: Mahmoud Amin (mahmoud.amin@manhattan.edu)

This work has been supported by Deanship of Scientific Research, Prince Sattam bin Abdulaziz University, Saudi Arabia, Under Grant Number (2017/ 01/ 7126).

ABSTRACT This paper presents a robust adaptive backstepping control (RABC) for high-speed permanent-magnet synchronous motor (HSPMSM) drive system. The proposed RABC achieves high performance operation by incorporating an ideal backstepping controller (IBC), a recurrent radial basis function neural network (RRBFNN) uncertainty observer, and a robust controller. The Lyapunov stability theorem is utilized to design the IBC as a position controller of the HSPMSM servo drive system. To enhance the disturbance rejection capability during parameter changes, certain information is needed within the backstepping control law so that the system performance would not sorely be affected. To mitigate the need for the lumped parameter uncertainties within the backstepping controller, an online adaptive observer based on RRBFNN is designed to estimate the nonlinear parameter uncertainties. Moreover, the robust controller is intended to retrieve the remaining of the RRBFNN approximation errors. To assure the stability of the proposed RABC, the Lyapunov stability analysis is used to derive the online adaptive control laws. The performance of the proposed RABC is verified by simulation and experimental analysis under different operating conditions and parameter uncertainties. The test results validate the effectiveness of the proposed RABC scheme to achieve preferable tracking performance regardless of external disturbances and parameter uncertainties.

INDEX TERMS Adaptive control, backstepping technique, Lyapunov stability theorem, high-speed permanent-magnet synchronous motor, radial basis function neural network (RBFNN), uncertainty observer.

I. INTRODUCTION

In recent years, several processing techniques of micro-electromechanical systems (MEMS) have been developed to reduce power dissipation, size, and weight of the micromotors. For special industrial applications, micromotors are considered good candidates to achieve high performance operation. The micro permanent-magnet synchronous motors (micro PMSMs) provide high efficiency, robustness, high power density, better reliability, and high speed operation compared to other micromotors [2], [3]. Furthermore, micro PMSMs are good nominees for several industrial applications such as medical diagnostic, surgical devices, security equipment, power driving devices in MEMS, and micro autonomic robots [4].

In the literature, several topologies and control techniques have been developed for micromotors [5]–[17]. In [5], a comparative analysis of inverter topologies for micromotors has

The associate editor coordinating the review of this manuscript and approving it for publication was Gaolin Wang.

been performed. A six-phase five-level inverter prototype was designed and tested at high frequency of 2 MHz. Various speed sensorless control techniques have been introduced for the micromotor drives [6]–[12]. For sensorless control of micro PMSMs, the rotor position measurement is estimated in the control schemes [6], [7]. A micro PMSM control system based on rotor position estimator and robust H_∞ controller was introduced in [8]–[10]. Several advanced control strategies for micromotors have been studied in [11] and [12]. For micro PMSM system in [13], a robust identifier and intelligent Petri-fuzzy neural network (PFNN) controller was proposed. An adaptive inverse control scheme incorporates an adaptive model for a micro PMSM drive system was developed [14]. In [15], an optimal design of sensorless-based speed controller of micro PMSM drives was proposed. Moreover, a motion controller involves a tuning parameter feed-forward function along with an optimal position controller was implemented for micro PMSM system [16]. In [17], a sliding-mode observer has been incorporated in a robust sensorless control method for high-speed micro PMSM.

Since micro PMSM drive system is extremely nonlinear, uncertain and has a wide range of operating conditions, the linearization around one operating point cannot be used to design the controller. To resolve this issue, nonlinear control techniques can be effectively utilized [18]–[21]. The recent development of backstepping control technique is a robust and consistent design approach for nonlinear feedback control schemes, which provides an option to conform the unmodeled and nonlinear impacts and parameter uncertainties. Several backstepping control design approaches have been suggested to handle nonlinear systems and motor drives [22]–[26]. The adaptive backstepping control approach is designed based on choosing recursively several proper functions of state variables as pseudo control inputs with reduced order subsystems of the whole control scheme. A new pseudo control structure from preceding stages is generated for each backstepping stage. The summation of all Lyapunov functions resulted from each design stage produces final Lyapunov function which fulfills the main design objective while terminating the actual control input of the feedback design. Therefore, favorable robustness features under parameter uncertainties are achieved using the backstepping control approach [18], [23]–[25].

Intelligent computation methodologies are attracting more attention due to rapid industrial developments. These methodologies have been evolved to enhance the drive system characteristics and to address the uncertainties and nonlinearities [27]–[34]. The architecture of the radial-basis function neural network (RBFNN) is designed based on the Kohonen network model. The RBFNN is structured of input, hidden, and output layers with normalized Gaussian activation functions. Although the simple structure of the RBFNN, it is one of the most preferable observers for position/speed controllers and nonlinear mapping problems due to its superior performance [35]–[40]. RBFNN has a quicker convergence feature than standard multilayer-perception neural network. RBFNN has a comparable characteristic as the fuzzy-logic scheme, in which the output result is studied employing the weighted-sum technique, and the number of nodes in the hidden layer is similar the fuzzy system structured of "if-then" rules. Furthermore, the RBFNN is represented by the field function which is the same as that of the fuzzy-logic system with its premise part constructed of the membership functions. Thus, the RBFNN can be incorporated effectively with nonlinear controllers designed for dynamic systems with parameter uncertainties since it introduces several features of its self-adaptation characteristics and numerous facets [40]. In [41], an improved performance of the shunt active power filter (APF) is accomplished by developing a radial basis function neural network (RBFNN) incorporated in an adaptive fuzzy-neural-network schematic. The proposed RBFNN is used to enhance the dynamic model of the APF through approximating its nonlinear function. Furthermore, the Lyapunov stability analysis is utilized to develop an online adaptive law in order to adjust the weights of the proposed RBFNN. In [42], a nonsingular terminal sliding mode backstepping (NTSMB) control approach is proposed to design an adaptive fuzzy-neural-network (AFNN) to mitigate the influence of the APF dynamic model uncertainties and external perturbations. In addition, the NTSMB robustness is enhanced by relieving the need of the preceding information of system specifications. In [43], the performance of the photovoltaic (PV)-based grid-connected single-phase inverter is improved using disturbance observer-based fuzzy sliding mode control (DOBFSMC) scheme. The proposed observer is utilized as an online estimator of system disturbances while the inverter output voltage is controlled using a sliding mode controller based on the information generated by the observer. Meanwhile, the system performance is enhanced through approximating the error value of the observer using fuzzy control system. Moreover, a terminal sliding-mode-based adaptive current controller for an APF is proposed [44]. To assure stable sliding surface properties with high accuracy, an adaptive finite-time fractional-order control scheme is designed. A fuzzy-neural observer is constructed to estimate the unknown nonlinearities of the APF while suppressing the current harmonic distortion. In [45], a robust adaptive vibration control is desired for systems with flexible risers subjected to input nonlinearities and unknown external disturbances. To eliminate the influence of input nonlinearities and limit the vibrational offset, a robust adaptive boundary controller is developed. Furthermore, the vibration control approach along with the adaptive upper-bound law is used to estimate the unknown disturbance boundary magnitude. In [46], another adaptive neural network based on backstepping approach is proposed to control a vibrating flexible string system. The effect of system uncertainties, input asymmetrical dead-region, and output restraint are considered. The proposed backstepping control strategy is designed to assure that the output constraints are not overridden. Meanwhile, the neural network is constructed to recover the input

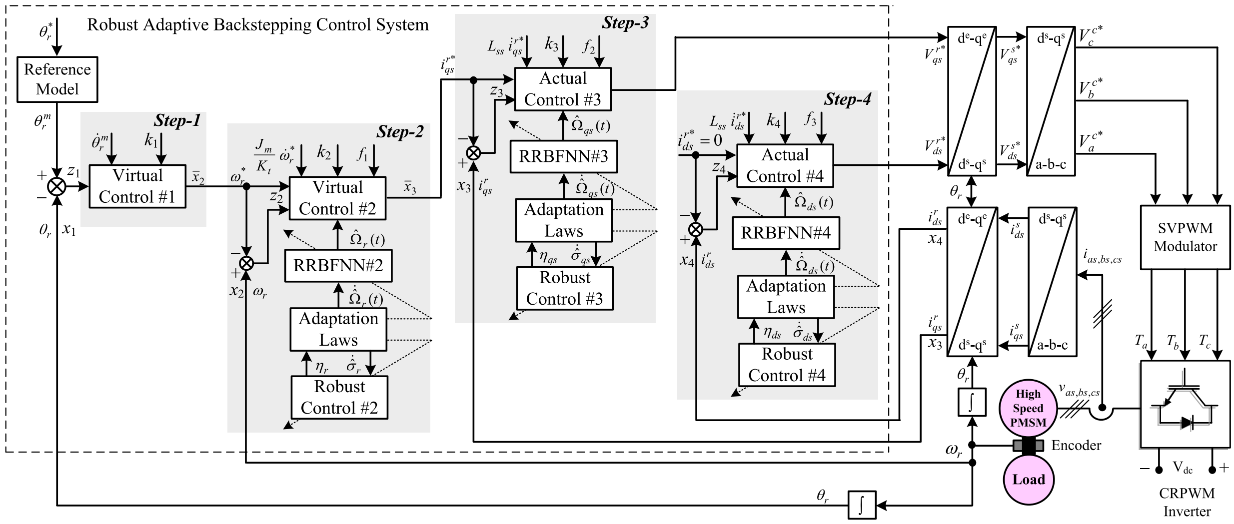

FIGURE 1. The proposed RABC framework for the HSPMSM drive system.

asymmetrical dead-region effect and maintain the overall string system stability. In [47], a new adaptive boundary control system is proposed to suppress the vibration of a belt system with axial movement and compensate for parametric disturbances. In addition, a disturbance observe is designed to mitigate the influence of the unknown boundary uncertainties. In [48], another boundary control scheme is desired to reduce the vibration of the flexible string system under the effect of external perturbations and input dead-region. The proposed scheme employs the backstepping control strategy to mitigate the vibration of the string system. Subsequently, the influence of the input dead-region is resolved using a RBFNN while the external perturbations are handled utilizing a disturbance observer.

This main contribution of this paper is to design a RABC scheme for the HSPMSM servo drive using an intelligent adaptive backstepping control system. The drive system structure of the designed RABC is demonstrated in Fig. 1. For industrial applications, the compounded disturbances and accurate lumped parameter uncertainties are harsh to be identified beforehand of the HSPMSM control operation. Thus, a novel scheme of nonlinear controller is considered here based on the adaptive backstepping control with RRBFNN to achieve the desired performance. Accordingly, the proposed control scheme incorporates three parts: an IBC, a RRBFNN-based uncertainty observer and a robust controller. Utilizing Lyapunov stability theorem, an effective design of the proposed RABC scheme is established to accurately control the rotor position of the HSPMSM drive system. Meanwhile, the uncertainty term existed in the backstepping control law is needed to be recognized as a mean to reduce the severe impact of the parameter changes on the system performance. The IBC can effectively control, track and regulate the rotor position of the drive system. Though, the drive system is still significantly affected by virtue of the existing uncertainties involving the unexpected disturbances, parameter variations, and inevitable approximation errors. This problem can be solved by using a RRBFNN uncertainty online observer to adaptively estimate the nonlinear parameter uncertainties. Furthermore, a robust controller is designed to retrieve the remaining of the relative errors of the RRBFNN. The Lyapunov stability analysis is used to assure the closed-loop system stability theory. The validity of the proposed RABC design is confirmed by test results (simulation and experimentation) subject tooled variations and parameter uncertainties. The test outcomes assure the effectiveness of the proposed RABC design through eliminating the external load perturbations in addition to compensating the parameter uncertainties.

Finally, the contributions of the proposed RABC scheme compared to other schemes are concluded as:

- The RRBFNN model has a new structure with the advantage of recurrent property which handles interim issues.
- The RRBFNN model has a quicker convergence feature than standard multilayer-perception NN.
- The RRBFNN model has a comparable characteristic as the fuzzy-logic scheme, in which the output result is studied employing the weighted-sum technique,
- The RRBFNN model has a hidden layer with number of nodes similar to the fuzzy system structured of "IF-THEN" rules.
- The RRBFNN model is represented by the field function which is the same as that of the fuzzy-logic system with its premise part constructed of the membership functions.
- The feedback of the output layer is added to accomplish faster convergence time.
- The RRBFNN neurons are susceptible to past data due to the self-connections of the hidden.

- Compared with RBFN, faster convergence and higher precision are achieved.
- In Section IV, it was validated that the proposed RABC with the RRBFNN uncertainty observer maintains robust control features and effectively controls the HSPMSM system under multiple perturbations and parameter uncertainties.

This paper is structured as: Section II introduces the HSPMSM dynamic modeling with parameter uncertainty and the problem description. In section III, the design procedure of the RABC scheme is presented. First, the structure of the RRBFNN uncertainty observer is provided. Then, the detailed design steps for the proposed IBC are also presented in this section. Moreover, the adaptive training methods and the stability study of the designed RABC scheme are illustrated in Section III. A development control board (dSPACE DS1102 DSP) is utilized to implement the proposed control algorithms. The HSPMSM servo system has been studied to examine the dynamic performance under two different conditions (extrinsic load perturbations and parameter uncertainties). Section IV provides the test results to confirm the validity of the proposed RABC design for the HSPMSM servo system. Finally, Section V introduces conclusions and summarizes the main contributions.

TABLE 1. The three-phase HSPMSM model parameters.

Parameter	Symbol	Value
Nominal power	P_n	1.2 W
Nominal torque	T_e	0.00044 N.m
Nominal speed	N_r	35940 rpm
Nominal voltage	$V_{L\text{-}L}$	12 V
Nominal current	I	0.105 A
Number of poles	P	2
Rotor inertia	J_m	$4.9\text{x}10^{-9}$ kg.m^2
Friction coefficient	β_m	$2\text{x}10^{-6}$N.m/rad/sec
Stator resistance	R_s	75.4 Ω
Voltage constant	λ_m	3474 rpm/V
Torque constant	K_t	0.00275 N.m/A

II. PROBLEM FORMULATION AND MATHEMATICAL PRELIMINARIES

A. THE HIGH-SPEED PMSM DYNAMIC MODEL WITH UNCERTAINTY

The field-oriented control (FOC) approach is applied with the aim of achieving high torque capability of the HSPMSM system by virtue of decoupling the $d-q$ axes stator currents in the rotor reference frame [18]. The motor parameters are denoted in Table 1. The analytical modeling of the HSPMSM in the rotating reference frame can be represented as:

$$V_{qs}^r = R_s i_{qs}^r + L_{ss}\frac{d}{dt}i_{qs}^r + \omega_r L_{ss} i_{ds}^r + \omega_r \lambda_m' \tag{1}$$

$$V_{ds}^r = R_s i_{ds}^r + L_{ss}\frac{d}{dt}i_{ds}^r - \omega_r L_{ss} i_{qs}^r \tag{2}$$

The electromagnetic torque can be represented by:

$$T_e = \frac{3}{2}\cdot\frac{P_n}{2}\cdot\lambda_m'\cdot i_{qs}^r = K_t i_{qs}^r \tag{3}$$

The HSPMSM motion dynamic equation can be described as:

$$T_e - T_L = J_m\left(2/P_n\right)\frac{d}{dt}\omega_r + \beta_m\left(2/P_n\right)\omega_r \tag{4}$$

where V_{qs}, V_{ds}, i_{qs} and i_{ds} are the $d-s$ tator voltages and currents. R_s and L_{ss} are the stator resistance and self-inductance. θ_r, ω_r, J_m, β_m and P are the rotor position, electrical rotor speed, effective inertia, friction coefficient and the number of poles of the HSPMSM, respectively. T_L and T_e are the load and electromagnetic torques, respectively. The torque constant is expressed as $K_t = (3/2)(P_n/2)\cdot\lambda_m'$.

It is common knowledge that the FOC of the HSPMSM enables an independent control of two input state variables, stator $d-q$-axis currents i_{ds}^r and i_{qs}^r. The dynamic model of the HSPMSM (1)-(4) in reliance on the field-oriented control in the synchronous reference frame [18] can be illustrated in state form as:

$$\begin{cases} \dot{\theta}_r = \omega_r \\ \dot{\omega}_r = \dfrac{K_t}{J_m}i_{qs}^r - \dfrac{1}{J_m}T_L - \dfrac{\beta_m}{J_m}\omega_r \\ \dot{i}_{qs}^r = -\dfrac{R_s}{L_{ss}}i_{qs}^r - \omega_r i_{ds}^r - \dfrac{1}{L_{ss}}\omega_r\lambda_m' + \dfrac{1}{L_{ss}}V_{qs}^r \\ \dot{i}_{ds}^r = -\dfrac{R_s}{L_{ss}}i_{ds}^r + \omega_r i_{qs}^r + \dfrac{1}{L_{ss}}V_{ds}^r \end{cases} \tag{5}$$

Due to temperature change, load disturbance, and saturation, the motor parameters are changing during motor operation. Thus, all these possible uncertainty factors should be considered during the design phase of the drive system controller. Accordingly, the perturbed dynamic model of the previous motor equations presented in (5) can be derived and expressed by (6)-(15) as follows:

$$\begin{cases} \dot{\theta}_r = \omega_r \\ (J_m + \Delta J_m)\dot{\omega}_r = (K_t + \Delta K_t)i_{qs}^r - (T_L + \Delta T_L) \\ -(\beta_m + \Delta\beta_m)\omega_r \\ (L_{ss} + \Delta L_{ss})\dot{i}_{qs}^r = -(R_s + \Delta R_s)i_{qs}^r - \omega_r i_{ds}^r \\ -\omega_r\lambda_m' + V_{qs}^r \\ (L_{ss} + \Delta L_{ss})\dot{i}_{ds}^r = -(R_s + \Delta R_s)i_{ds}^r + \omega_r i_{qs}^r + V_{ds}^r \end{cases} \tag{6}$$

$$\begin{cases} \dot{\theta}_r = \omega_r \\ J_m\dot{\omega}_r = K_t i_{qs}^r - (T_L + \Delta T_L) - \beta_m\omega_r \\ +\left(f_r - \Delta J_m\dot{\omega}_r - \Delta\beta_m\omega_r + \Delta K_t i_{qs}^r - \Delta T_L - T_L\right) \\ L_{ss}\dot{i}_{qs}^r = -R_s i_{qs}^r - \omega_r i_{ds}^r - \omega_r\lambda_m' + V_{qs}^r \\ +\left(f_{qs} - \Delta L_{ss}\dot{i}_{qs}^r - \Delta R_s i_{qs}^r + \Delta L_{ss}\omega_r i_{ds}^r\right) \\ L_{ss}\dot{i}_{ds}^r = -R_s i_{ds}^r + \omega_r i_{qs}^r + V_{ds}^r \\ +\left(f_{ds} - \Delta L_{ss}\dot{i}_{ds}^r - \Delta R_s i_{ds}^r + \Delta L_{ss}\omega_r i_{ds}^r\right) \end{cases} \tag{7}$$

The state vector and its derivative are given by:

$$x = \begin{bmatrix} x_1 \\ x_2 \\ x_3 \\ x_4 \end{bmatrix} = \begin{bmatrix} \theta_r \\ \omega_r \\ i_{qs}^r \\ i_{ds}^r \end{bmatrix}, \quad \dot{x} = \begin{bmatrix} \dot{x}_1 \\ \dot{x}_2 \\ \dot{x}_3 \\ \dot{x}_4 \end{bmatrix} = \begin{bmatrix} \dot{\theta}_r \\ \dot{\omega}_r \\ \dot{i}_{qs}^r \\ \dot{i}_{ds}^r \end{bmatrix} \tag{8}$$

Using (6)-(8), the perturbed dynamical model of the HSPMSM is expressed in the following form:

$$\dot{x}_1 = \dot{\theta}_r = x_2 \tag{9}$$

$$\dot{x}_2 = \dot{\omega}_r = -\frac{\beta_m}{J_m}x_2 + \frac{K_t}{J_m}x_3 + \Omega_r \tag{10}$$

$$\dot{x}_3 = \dot{i}^r_{qs} = -\frac{R_s}{L_{ss}}x_3 - x_2x_4 - \frac{\lambda'_m}{L_{ss}}x_2 + \frac{V^r_{qs}}{L_{ss}} + \Omega_{qs} \tag{11}$$

$$\dot{x}_4 = \dot{i}^r_{ds} = -\frac{R_s}{L_{ss}}x_4 + x_2x_3 + \frac{V^r_{ds}}{L_{ss}} + \Omega_{ds} \tag{12}$$

and the uncertainty terms in (10)-(12) are given by (13)-(15):

$$\Omega_r = \frac{1}{J_m}\left(f_r - \Delta J_m\dot{x}_2 - \Delta\beta_m x_2 + \Delta K_t x_3 - \Delta T_L - T_L\right) \tag{13}$$

$$\Omega_{qs} = \frac{1}{L_{ss}}\left(f_{qs} - \Delta L_{ss}\dot{x}_3 - \Delta R_s x_3 + \Delta L_{ss}x_2x_4\right) \tag{14}$$

$$\Omega_{ds} = \frac{1}{L_{ss}}\left(f_{ds} - \Delta L_{ss}\dot{x}_4 - \Delta R_s x_4 + \Delta L_{ss}x_2x_4\right) \tag{15}$$

where Ω_r, Ω_{qs} and Ω_{ds} represent the lumped parameter uncertainties, wherein ΔR_s, ΔL_{ss}, ΔK_t, $\Delta\beta_m$, ΔJ_m and ΔT_L denote possible uncertainties in the drive system parameters; f_r, f_{qs} and f_{ds} are added to indicate the extrinsic perturbations in realistic applications. The lumped parameter limits of the possible uncertainties are expressed by $|\Omega_r| < \delta_r$, $\left|\Omega_{qs}\right| < \delta_{qs}$ and $|\Omega_{ds}| < \delta_{ds}$; δ_r, δ_{qs} and δ_{ds} are positive constants.

Remark 1: In the dynamic modeling of the motor formulated by (9)-(15) encompasses all uncertainties, the presence of nonlinearities is explicit due to the $d-q$ stator current, the compounded rotor speed, and the permanent flux terms. Furthermore, there occur irregularities as a result of the nonlinear features of the CRPWM inverter. This is a substantial cause of the design difficulty for the robust control of HSPMSM system. Besides, the parameter variations enlarge the nonlinearities and reduce the system performance or even demolish the control stability. To design a superior control of the motor drive system, particular factors such as the system nonlinearities, parameter changes and extrinsic load perturbations should be canceled or restricted within an attenuation level. Favorably, the whole nonlinear reliance might be intended into the parameter uncertainties (13)-(15) and the proposed controller need to be designed robust adequate to with stand un-modeled dynamics as well as these uncertainties.

Assumption 1: The HSPMSM states, $x_1 = \theta_r$, $x_2 = \omega_r$, $x_3 = i^r_{qs}$ and $x_4 = i^r_{ds}$, are measurable since the backstepping control scheme requires these feedback signals.

B. PROBLEM DESCRIPTION

The proposed RABC framework for the HSPMSM system is shown in Fig. 1. The drive system contains a HSPMSM, a three-phase current regulated pulse width modulation (CRPWM) inverter and the load. The system uncertainties exist in the perturbed dynamic model of the HSPMSM drive system (9)-(12) are presumed to be limited. These uncertainties include extrinsic perturbations as well as unknown modeling inaccuracies. From (13)-(15), it is noticed that the terms of uncertainty cannot be directly evaluated. Subsequently, the RRBFNN-based uncertainty observer is proposed to estimate the nonlinear lumped parameter uncertainty terms for the HSPMSM drive system. The control objective is to develop a robust adaptive backstepping control (RABC) system with RRBFNN uncertainty observer such that the closed-loop system of (9)-(12) is stable in the existence of parameter uncertainties and extrinsic perturbations. Eventually, all errors are consistently restricted and the tracking error value can be arbitrary small as $t \to \infty$. The configuration of the designed RABC is shown in Fig. 1.

In this paper, a novel RABC scheme is designed to control the HSPMSM drive system. The proposed scheme integrates IBC, RRBFNN-based uncertainty observer and robust controller. First, the mathematical model of the HSPMSM with parameter variations and external disturbances is derived. The FOC approach is utilized here to enhance the dynamic performance of the drive system through the decoupling control property. In accordance with the backstepping process, an IBC is designed based on Lyapunov stability theorem to fulfill several goals of a persistent rotor position while tracing the desired trajectory. Though, accurate data about the lumped parameter uncertainties of the drive system are needed within the backstepping control law in such a way the performance would not sorely affected. To mitigate the need for the parameter uncertainties within the IBC structure, an online adaptive observer based on RRBFNN is intended to evaluate the nonlinear parameter uncertainties. Furthermore, the robust controller is configured to retrieve the remaining of the RRBFNN estimate error. To ensure the stability of the proposed RABC, the Lyapunov stability analysis is employed to obtain the online adaptive control laws.

III. ROBUST ADAPTIVE BACKSTEPPING CONTROL VIA RRBFNN UNCERTAINTY OBSERVER

The main idea of the backstepping process is to structure a new subsystem using preselected state variable that needed to be stabilized. Therefore, the error functions of the new state variables are chosen to be attenuated to zero. As a result, a virtual control law is derived by selecting a proper Lyapunov candidate function. Eventually, an actual control law could be concluded, and the proposed system stability would be assured. In this section, the structure of the designed RABC for the HSPMSM is presented. At the nominal parameters, the IBC can fulfill a desirable performance of the HSPMSM position control. Nevertheless, the control performance of the HSPMSM is still susceptible to parameter changes. To resolve this issue with an effective control design of the rotor position of the HSPMSM, a RABC is developed here. The structure of the designed RABC system, which incorporates an IBC, a RRBFNN uncertainty observer and a robust controller, is shown in Fig. 1.

A. RRBFNN UNCERTAINTY OBSERVER

The HSPMSM drive system involving parameter uncertainties is expressed in terms of the unknown nonlinear parameter

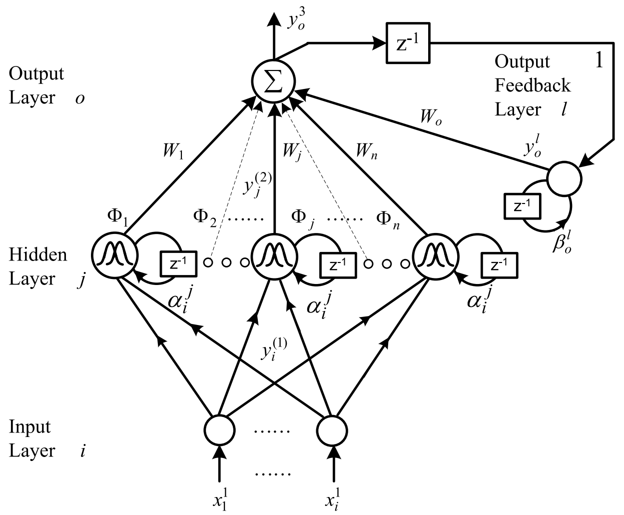

FIGURE 2. **Recurrent radial basis function neural network (RRBFNN).**

uncertainty function which can be estimated here using the proposed RRBFNN uncertainty observer. To adaptively estimate this nonlinear dynamic function, $\hat{\Omega}(\cdot)$, the backpropagation algorithm is utilized to train the RRBFNN. To implement the proposed uncertainty observer, a three-layer RRBFNN is suggested here to optimize the precision of the function approximation. The proposed RRBFNN encompasses three-layers, two inputs (the i layer), hidden (the j layer), and one output (the o layer), as shown in Fig. 2. In addition, the Gaussian function is selected as the particular field function in the hidden layer due to its differential and persistent characteristics. Furthermore, the RRBFNN output is repeated to the input of the output layer with a time delay. The basic function and signal propagation in each layer of the proposed RRBFNN are expressed as shown below [18]:

Layer 1: Input Layer

Layer 1 involves some nodes to transmit the input signals to the subsequent layer. In the input layer, every input and output node i of the RRBFNN can be expressed as:

$$net_i^1 = x_i^1(N) \tag{16}$$

$$y_i^1(N) = f_i^1(net_i^1(N)) = net_i^1(N), \quad i = 1, \cdots, m \tag{17}$$

where x_i^1 illustrates the ith input to the node of layer 1 and N indicates the number of iterations.

Layer 2: Hidden Layer

Every node in the hidden layer precedes a susceptible field function. The Gaussian function is chosen as the receptive field function in the hidden layer due to its differential and persistent features. For the jth hidden node:

$$net_j^2(N) = -(\mathrm{X}-\mu_j)^T\sigma_j(\mathrm{X}-\mu_j) + \Phi_j(N-1)\alpha_j \tag{18}$$

$$y_j^2(N) = f_j^2(net_j^2(N)) = \exp(net_j^2(N)), \quad j = 1, \ldots, n \tag{19}$$

where the standard deviation and mean vectors of the Gaussian functions are $\sigma_j = [1/\sigma_{1j}^2, 1/\sigma_{2j}^2, \ldots, 1/\sigma_{ij}^2]^T$ and $\mu_j = [\mu_{1j}, \mu_{2j}, \ldots, \mu_{ij}]^T$, respectively, μ_{ij} and σ_{ij} are the standard deviation and mean of the jth neuron in the hidden layer of the ith input of the RRBFNN, n indicates the number of receptive field units and bases in the hidden layer, $\mathrm{X} = [x_1, x_2, \ldots, x_i]^T \in \Re^{m\times 1}$ is the input vector of the input layer, $\Phi = [\Phi_1, \Phi_2, \ldots, \Phi_j, \Phi_n]^T \in \Re^{n\times 1}$ is the output vector of the hidden layer, $0 \le \alpha < 1$ is the self-connecting feedback gain of the hidden layer.

Layer 3: Output Layer

The single node o in the output layer is represented by $\sum$, which calculates the total output as the addition of all arriving signals to acquire the final outcomes.

$$net_o^3 = \sum\nolimits_j W_j y_j^2(N) + W_o y_o^l \tag{20}$$

$$y_o^3(N) = f_o^3(net_o^3(N)) = net_o^3(N)o = 1 \tag{21}$$

$$\Phi_j(N) = \exp\left(-(\mathrm{X}-\mu_j)^T\sigma_j(\mathrm{X}-\mu_j)+\Phi_j(N-1)\alpha_j\right) \tag{22}$$

$$y_o^l(N) = y_o^l(N-1)\beta_j + y_o^3(N-1) \tag{23}$$

$$y_o^3 = \hat{\Omega}(\cdot) \tag{24}$$

where $W_j = [\varpi_1, \varpi_2, \ldots, \varpi_j, \varpi_n]^T \in \Re^{n\times 1}$ is the adaptable weight vector between the hidden and the output layers, $W_o = [\varpi_o]^T \in \Re^{1\times 1}$ is the connective weight of output feedback neuron to output neuron, y_o^l is the feedback layer output, $y_o^3 = \hat{\Omega}(\cdot)$ is the output of the RRBFNN, $0 \le \beta < 1$ is the self-connecting feedback gain of the output layer, $\hat{\Omega}(\cdot)$ is the function of the nonlinear parameter uncertainty. For the uncertainty estimation, the vector form of the RRBFNN output can be expressed as:

$$y_o^3(x, \sigma, \mu, \alpha, \beta, W) = W^T\Phi(x, \sigma, \mu, \alpha, \beta) \tag{25}$$

where W is the weight vector and Φ is the firing strength vector. Even for time-varying function, it was confirmed that an RRBFNN exists as shown in (25) such that it can symmetrically approximate function nonlinearity [40].

Assumption 2: consider the RRBFNN input, $X = [x_1, x_2, \ldots, x_i]^T$, pertains to a compact set κ_X and the RRBFNN is utilized to estimate the nonlinear function $\Omega(X)$. The optimal parameter vector of the proposed RRBFNN, W^*, is provided by [51]–[54]:

$$W_k^* = \arg\min_{\hat{W}\in\kappa_W}\left[\sup_{X\in\kappa_X}\left\|\Omega_k(X) - \hat{\Omega}_k(X\left|\hat{W}_k\right.)\right\|\right] \tag{26}$$

It is presumed that the optimal parameter vector, W_k^*, is limited to a compact set of the parameter vector, κ_W.

B. ONLINE LEARNING ALGORITHM

The parameter learning algorithm is used to adjust the parameters of the RRBFNN bases, feedback weight and the connection weight (μ, σ, α, βW_j and W_o) optimally with the same training pattern. The detailed derivation of the learning methodology is given in the Appendix. In this paper, the weights, W_j, W_o, α_i^j, and β_o^l as well as the mean μ_i^j, and the standard deviation σ_i^j, are under training to get the adapted laws using Lyapunov stability. The weighting vector W which collects all weights for training, is defined as

$$
\begin{aligned}
W &= [W_j, W_o, \alpha, \beta, \mu, \sigma] \\
&= \begin{bmatrix}
(w_{11}, \cdots, w_{n_m 1}, \ldots, w_{12}, \ldots, w_{n_m 2}, \cdots, \\
w_{1n_j}, \cdots, w_{n_m n_j}), \\
(w_{1l}, \cdots, w_{n_m 1l}, \ldots, w_{2l}, \ldots, w_{n_m 2l}, \cdots, \\
w_{1n_l}, \cdots, w_{n_m n_l}), \\
(\alpha_{1j}, \alpha_{2j}, \ldots, \alpha_{mj}, \ldots, \alpha_{n_m j}), \\
(\beta_{1l}, \beta_{2l}, \ldots, \beta_{ml}, \ldots, \beta_{n_m l}), \\
(\mu_{11}, \cdots, \mu_{n_i 1}, \ldots, \mu_{12}, \ldots, \mu_{n_i 2}, \cdots, \\
\mu_{1n_j}, \cdots, \mu_{n_i n_j}), \\
(\sigma_{11}, \cdots, \sigma_{n_i 1}, \ldots, \sigma_{12}, \ldots, \sigma_{n_i 2}, \cdots, \\
\sigma_{1n_j}, \cdots, \sigma_{n_i n_j}).
\end{bmatrix}
\end{aligned}
$$

C. CONVERGENCE ANALYSES

In this paper, the convergence analyses are introduced to derive the learning rates parameters to assure convergence of the output error of RRBFNN parameters. Therefore, the learning rates parameters selection has a significant effect on the RRBFNN performance. In order to train the RRBFNN effectively, six varied learning rates, $\eta_W, \eta_o \eta_\mu, \eta_\sigma, \eta_\beta$ and η_α, which guarantee the convergence of tracking errors and identification based on the analyses of a discrete-type Lyapunov function, are derived in the Appendix [27], [49], [50].

D. THE PROPOSED RABC SYSTEM DESIGN

The main goal of this paper is to design a robust and efficient control method for the HSPMSM model described by (9)-(15) regardless load disturbances and obscure parameter changes. Accordingly, an RABC scheme employing the RRBFNN-based uncertainty observer was designed as shown in Fig. 1.Thus, the rotor position state trajectory $\theta_r(t)$ can asymptotically follow the reference state trajectory position $\theta_r^*(t)$.We presume that $\theta_r^*(t)$ and $\dot{\theta}_r^*(t)$ are the time functions with additional constraints.

To accurately detect the lumped parameter uncertainties described in (13)-(15), the RRBFNN-based observer outputs $\hat{\Omega}_r(\cdot)$, $\hat{\Omega}_{qs}(x_{qs})$ and $\hat{\Omega}_{ds}(x_{ds})$ are derived according to assumption 1 and the universal approximation theorem in [51], [52] as:

$$\Omega_k(x_k) = W_k^{*T} \Phi_k^* + \varepsilon_k \tag{27}$$

where W_k^* and Φ_k^* represent the optimal parameter matrices of the proposed observer while $k = r, qs, ds$; ε_k is the minimum remodeled error. Although these optimal parameter matrices cannot be obtained, although, it can be estimated using the RRBFNN uncertainty observer as:

$$\hat{\Omega}_k(x_k) = \hat{W}_k^T \hat{\Phi}_k + u_k^{RC} \tag{28}$$

where $\hat{W}_k$ and $\hat{\Phi}_k$ are the estimated values of the optimal parameter matrices W_k^* and Φ_k^*, respectively; u_k^{RC} expresses the robust controller function that recover the flaw of the proposed RRBFNN uncertainty observer as a result of tracking, weight, and estimation errors. The parameter uncertainties in (13)-(15) can be illustrated as:

$$
\begin{aligned}
\Omega_k(x_k \left| W_k^* \right.) &= \Omega_k^*(x_k \left| W_k^* \right.) + \varepsilon_k \\
&= \hat{\Omega}_k(x_k \left| \hat{W}_k \right.) + \left[\Omega_k^*(x_k \left| W_k^* \right.) - \hat{\Omega}_k(x_k \left| \hat{W}_k \right.) \right] \\
&\quad + \varepsilon_k + u_k^{RC}
\end{aligned} \tag{29}
$$

where $\hat{W}_k$ and W_k^* are the estimated and optimal weight matrices, respectively. $x_r = (x_1, x_2, \dot{x}_1)$, $x_{qs} = (x_1, x_2, x_3, \dot{x}_2)$ and $x_{ds} = (x_1, x_2, x_3, \dot{x}_3)$ are the inputs to the RRBFNNs.

Assumption 3: Presume that W_k^* matrices are limited as $\left\| W_k^* \right\|_F \le W_{k,M}$, where $\|\cdot\|_F$ indicates the Frobenius norm [51], [52].

It is noticed that the restricted values $W_{k,M}$ are not needed to carry out the designed control system. However, those values are still necessary to perform the stability analysis. The weights of the RRBFNN uncertainty observer can be trained through applying the Taylor series expansion of $\Omega_k^*(x_k \left| W_k^* \right.)$ around $\left| \hat{W}_k \right.$. Thus, the error function can be optimized as [51]–[57]:

$$
\begin{aligned}
&\Omega_k^*(x_k \left| W_k^* \right.) - \hat{\Omega}_k(x_k \left| \hat{W}_k \right.) \\
&\quad = \tilde{W}_k^T \Xi_k + H_k(W_k^*, \hat{W}_k)
\end{aligned} \tag{30}
$$

$$\Xi_k = \left[\frac{\partial \hat{\Omega}_{k,1}}{\partial \hat{W}_{k,1}}, \frac{\partial \hat{\Omega}_{k,2}}{\partial \hat{W}_{k,2}}, \cdots, \frac{\partial \hat{\Omega}_{k,n}}{\partial \hat{W}_{k,n}}, \right]^T \tag{31}$$

where $k = r, qs, ds$ and the vectors with higher order terms are represented by $\tilde{W}_k = (W_k^* - \hat{W}_k)$ and $H_k(W_k^*, \hat{W}_k)$. Substituting (30) into (31) will provide:

$$\Omega_k(x_k \left| W_k \right.) = \hat{\Omega}_k(x_k \left| \hat{W}_k \right.) + \tilde{W}_k^T \Xi_k + \gamma_k - u_k^{RC} \tag{32}$$

where $\gamma_k = H_k(W_k^*, \hat{W}_k) + \varepsilon_k$. The uncertainty expression γ_k is presumed to be limited by $\|\gamma_k\| \le \sigma_k$ while σ_k are positive constants. Due to the uncertainty observer errors (tracking, estimation, and weight), we can use σ_k to represent the flaw of the proposed RRBFNN design. Rewrite (32) will provide:

$$\Omega_k(x_k \left| W_k \right.) = \hat{\Omega}_k(x_k \left| \hat{W}_k \right.) + \tilde{W}_k^T \Xi_k + \gamma_k - u_k^{RC} \tag{33}$$

The design procedures of the overall proposed RABC system including the RRBFNN uncertainty observer are summarized as follows:

Procedure 1: Determine the state function of the tracking error:

$$z_1(t) = \theta_r(t) - \theta_r^m(t) \tag{34}$$

Thereafter, by differentiating the error function as:

$$\dot{z}_1(t) = \dot{\theta}_r(t) - \dot{\theta}_r^m(t) = \omega_r - \dot{\theta}_r^m(t) \tag{35}$$

where $\dot{\theta}_r(t) = \omega_r(t)$ can be noted as virtual control in (35). A Lyapunov function nominee can be adopted as:

$$V_1(t) = \frac{1}{2} z_1^2(t) \tag{36}$$

By differentiating (36) then substituting from (35) as:

$$\dot{V}_1(t) = z_1\dot{z}_1 = z_1[\dot{\theta}_r(t) - \dot{\theta}_r^m(t)] \quad (37)$$

Subsequently, set the virtual control law $\bar{x}_2(t) = \omega_r^*$ as follows:

$$\bar{x}_2 = -k_1 z_1(t) + \dot{\theta}_r^m(t) \quad (38)$$

where $k_1 > 0$ is defined as again value for the control design.

Procedure 2: Repeat procedure 1 through defining the tracking error state function of the rotor speed:

$$z_2(t) = x_2(t) - \omega_r^*(t) \quad (39)$$

Therefore, by utilizing (10) and (27)-(29), the error function is differentiated as:

$$\begin{aligned}\dot{z}_2(t) &= \dot{x}_2 - \dot{\omega}_r^*(t)\\ &= -(\beta_m/J_m)x_2 + (K_t/J_m)x_3 + \Omega_r - \dot{\omega}_r^*(t)\\ &= f_1 + (K_t/J_m)x_3 + \Omega_r - \dot{\omega}_r^*(t) \quad (40)\end{aligned}$$

where $f_1 = -(\beta_m/J_m)x_2$.
The candidate of the Lyapunov function is selected as:

$$V_2(t) = V_1(t) + \frac{1}{2}z_2^2(t) \quad (41)$$

By differentiating $V_2(t)$ then utilizing (39) and (40):

$$\begin{aligned}\dot{V}_2(t) &= \dot{V}_1(t) + z_2(t)\dot{z}_2(t)\\ &= -k_1 z_1^2 + z_2(t)\left(-\frac{\beta_m}{J_m}x_2 + \frac{K_t}{J_m}x_3 + \Omega_r - \dot{\omega}_r^*(t)\right) \quad (42)\end{aligned}$$

The virtual control law $\bar{x}_3(t) = i_{qs}^{r*}$ is constructed as:

$$\begin{aligned}\bar{x}_3 &= (J_m/K_t)\left(-k_2 z_2 - f_1 - \hat{\Omega}_r + \dot{\omega}_r^*(t)\right)\\ &= (J_m/K_t)\left(-k_2 z_2 - f_1 - \hat{W}_r^T\,\Xi_r - u_r^{RC} - \sigma_r + \dot{\omega}_r^*(t)\right) \quad (43)\end{aligned}$$

where $k_2 > 0$ is defined as a design control gain; the estimated value of the approximated parameter uncertainty Ω_r of the RRBFNN-based observer is defined as $\hat{\Omega}_r = \hat{W}_r^T\,\Xi_r + u_r^{RC} + \sigma_r$. Thus, the tracking error state of the rotor speed can be defined as:

$$z_3(t) = x_3(t) - \bar{x}_3(t) \quad (44)$$

Procedure 3: The derivative of (44) and employing (11) as:

$$\begin{aligned}\dot{z}_3(t) &= \dot{x}_3(t) - \dot{\bar{x}}_3(t)\\ &= -\frac{R_s}{L_{ss}}x_3 - x_2x_4 - \frac{\lambda_m'}{L_{ss}}x_2 + \frac{V_{qs}^r}{L_{ss}} + \Omega_{qs} - \dot{i}_{qs}^{r*}(t)\\ &= f_2 + \frac{V_{qs}^r}{L_{ss}} + \Omega_{qs} - \dot{i}_{qs}^{r*}(t) \quad (45)\end{aligned}$$

where $f_2 = (L_{ss})^{-1}\left(-R_s x_3 - x_2 x_3 L_{ss} - \lambda_m' x_2\right)$.
Select the candidate of the Lyapunov function to be:

$$V_3(t) = V_2(t) + \frac{1}{2}z_3^2(t) \quad (46)$$

Moreover, the derivative of (46) will introduce:

$$\begin{aligned}\dot{V}_3(t) &= \dot{V}_2(t) + z_3(t)\dot{z}_3(t)\\ &= -k_2 z_2^2 + z_3(t)\left(f_2 + (V_{qs}^r/L_{ss}) + \Omega_{qs} - \dot{i}_{qs}^{r*}(t)\right) \quad (47)\end{aligned}$$

The q-axis desired control law V_{qs}^{r*} is prepared as:

$$\begin{aligned}V_{qs}^{r*} &= L_{ss}\left(-k_3 z_3 - f_2 - \hat{\Omega}_{qs} + \dot{i}_{qs}^{r*}(t)\right)\\ &= L_{ss}\left(-k_3 z_3 - f_2 - \hat{W}_{qs}^T\,\Xi_{qs} - u_{qs}^{RC} - \sigma_{qs} + \dot{i}_{qs}^{r*}(t)\right) \quad (48)\end{aligned}$$

where $k_3 > 0$ is defined as a design control gain; the q-axis estimated value of the approximated parameter uncertainty Ω_{qs} of the RRBFNN-based observer is defined as $\hat{\Omega}_{qs} = \hat{W}_{qs}^T\,\Xi_{qs} + u_{qs}^{RC} + \sigma_{qs}$.Thus, the state function of the tracking error can be determined as:

$$z_4(t) = x_4(t) - i_{ds}^{r*}(t) \quad (49)$$

Procedure 4: By using the derivative of (49) then substituting from (12) yields:

$$\begin{aligned}\dot{z}_4(t) &= \dot{x}_4(t) - \dot{i}_{ds}^{r*}(t)\\ &= f_3 + \frac{V_{ds}^r}{L_{ss}} + \Omega_{ds} - \dot{i}_{ds}^{r*}(t) \quad (50)\end{aligned}$$

where $f_3 = -(R_s/L_{ss})x_4 + x_2x_3$.
Subsequently, select the candidate of the Lyapunov function as:

$$V_4(t) = V_3(t) + \frac{1}{2}z_4^2(t) \quad (51)$$

Thereafter, (51) is differentiated and substituting from (47) as:

$$\begin{aligned}\dot{V}_4(t) &= \dot{V}_3(t) + z_4(t)\dot{z}_4(t)\\ &= -k_3 z_3^2 + z_4(t)\left(f_3 + \frac{V_{ds}^r}{L_{ss}} + \Omega_{ds} - \dot{i}_{ds}^{r*}(t)\right) \quad (52)\end{aligned}$$

The d-axis desired control law V_{ds}^{r*} is derived as:

$$\begin{aligned}V_{ds}^{r*} &= L_{ss}\left(-k_4 z_4 - f_3 - \hat{\Omega}_{ds} + \dot{i}_{ds}^{r*}(t)\right)\\ &= L_{ss}\left(-k_4 z_4 - f_3 - \hat{W}_{ds}^T\,\Xi_{ds} - u_{ds}^{RC} - \sigma_{ds} + \dot{i}_{ds}^{e*}(t)\right) \quad (53)\end{aligned}$$

where $k_4 > 0$ is a defined as a design control gain; the d-axis estimated value of the approximated parameter uncertainty Ω_{ds} of the RRBFNN-based observer is defined as $\hat{\Omega}_{ds} = \hat{W}_{ds}^T\,\Xi_{ds} + u_{ds}^{RC} + \sigma_{ds}$.

E. STABILITY ANALYSIS OF THE PROPOSED RABC SYSTEM

This section aims to examine the stability analysis of the proposed RABC process with a RRBFNN-based uncertainty observer for the motor drive system operation. The candidate of the Lyapunov function can be considered as follows:

$$\begin{aligned}V_a &= \frac{1}{2}\sum_{\upsilon=1}^{3} z_\upsilon^T z_\upsilon + \frac{1}{2\eta_r}\mathrm{tr}(\tilde{W}_r^T\Gamma_r^{-1}\tilde{W}_r^T) + \frac{1}{2\eta_{qs}}\mathrm{tr}(\tilde{W}_{qs}^T\Gamma_{qs}^{-1}\tilde{W}_{qs}^T)\\ &\quad + \frac{1}{2\eta_{ds}}\mathrm{tr}(\tilde{W}_{ds}^T\Gamma_{ds}^{-1}\tilde{W}_{ds}^T) + \frac{1}{2\eta_r}\Gamma_r^{-1}\tilde{\sigma}_r^2 + \frac{1}{2\eta_{qs}}\Gamma_{qs}^{-1}\tilde{\sigma}_{qs}^2\\ &\quad + \frac{1}{2\eta_{ds}}\Gamma_{ds}^{-1}\tilde{\sigma}_{ds}^2 \quad (54)\end{aligned}$$

where $\Gamma_{qs} = \mathrm{diag}[\Gamma_{qs,i}]$, $\Gamma_{qs} = \mathrm{diag}[\Gamma_{qs,i}]$, and $\Gamma_{ds} = \mathrm{diag}[\Gamma_{ds,i}]$, $i = [1, 2, \cdots, n]$, and $\Gamma_{r,i}$, $\Gamma_{qs,i}$, and $\Gamma_{ds,i}$ are the tuning gains. $\mathrm{tr}(\cdot)$ indicates the trace of a matrix.

Assumption 4: Suppose that ξ is positive constant and the Lyapunov function candidate denoted in (54) is limited as $V_a \leq \xi$.

Stability Theorem: The HSPMSM drive system is demonstrated by (9)-(15) while uncertainties are considered. The adaptive control laws, represented by (38), (43), (48) and (53), are used to design the proposed RABC with a RRBFNN-based uncertainty observer. Furthermore, if the control system fulfills Assumptions (1-4) and the adaptation control laws are selected as (55)-(57) for all weights of the RRBFNN observer, then the stability of the designed RABC can be ensured via designing the robust controllers as (58)-(60) with the adaptive estimations to be limited as (61)-(63).

$$\dot{\hat{W}}_{r,i} = \Gamma_{r,i}\Xi_{r,i}z_{2,i} - \eta_r\Gamma_{r,i}\hat{W}_{r,i} \tag{55}$$
$$\dot{\hat{W}}_{qs,i} = \Gamma_{qs,i}\Xi_{qs,i}z_{3,i} - \eta_{qs}\Gamma_{qs,i}\hat{W}_{qs,i} \tag{56}$$
$$\dot{\hat{W}}_{ds,i} = \Gamma_{ds,i}\Xi_{ds,i}z_{4,i} - \eta_{ds}\Gamma_{ds,i}\hat{W}_{ds,i} \tag{57}$$
$$u_{r,i}^{RC} = \hat{\sigma}_{r,i}\mathrm{sgn}(z_{2,i}) \tag{58}$$
$$u_{qs,i}^{RC} = \hat{\sigma}_{qs,i}\mathrm{sgn}(z_{3,i}) \tag{59}$$
$$u_{ds,i}^{RC} = \hat{\sigma}_{ds,i}\mathrm{sgn}(z_{4,i}) \tag{60}$$
$$\dot{\hat{\sigma}}_{r,i} = \eta_r\left|(z_{2,i})\right| \tag{61}$$
$$\dot{\hat{\sigma}}_{qs,i} = \eta_{qs}\left|(z_{3,i})\right| \tag{62}$$
$$\dot{\hat{\sigma}}_{ds,i} = \eta_{ds}\left|(z_{4,i})\right| \tag{63}$$

where η_r, η_{qs} and η_{ds} are positive constants; $\Xi_{r,i}$, $\Xi_{qs,i}$ and $\Xi_{ds,i}$ are the ith elements of Ξ_r, Ξ_{qs} and Ξ_{ds}, respectively. σ_r, σ_{qs} and σ_{ds} represent the terms of uncertainty which can be estimated online by $\hat{\sigma}_r$, $\hat{\sigma}_{qs}$ and $\hat{\sigma}_{ds}$, respectively. The $\mathrm{sgn}(\cdot)$ indicates the sign function. Eventually, upon satisfying Assumption 4 with any initial conditions, the adjustable weights $\dot{\hat{W}}_{r,i}$, $\dot{\hat{W}}_{qs,i}$ and $\dot{\hat{W}}_{ds,i}$ and the errors of states $Z = [z_1, z_2, z_3, z_4]$ of the closed loop system are symmetrically restricted and can be maintained at arbitrary small value.

Proof of Stability Theorem:

The tracking error states can be differentiated as $\dot{Z} = [\dot{z}_1, \dot{z}_2, \dot{z}_3, \dot{z}_4]$ by substituting (38), (43), (48) and (53) into(35), (40), (45) and (50), respectively, as follows:

$$\dot{z}_1(t) = -k_1z_1 \tag{64}$$
$$\dot{z}_2(t) = -k_2z_2 + \tilde{W}_r^T\Xi_r + \sigma_r - u_r^{RC} \tag{65}$$
$$\dot{z}_3(t) = -k_3z_3 + \tilde{W}_{qs}^T\Xi_r + \sigma_{qs} - u_{qs}^{RC} \tag{66}$$
$$\dot{z}_4(t) = -k_4z_4 + \tilde{W}_{ds}^T\Xi_{ds} + \sigma_{ds} - u_{ds}^{RC} \tag{67}$$

If we differentiate the candidate of the Lyapunov function (54) and utilizing (64)-(67), we will attain the following:

$$\begin{aligned}\dot{V}_a &= z_1^T\dot{z}_1 + z_2^T\dot{z}_2 + z_3^T\dot{z}_3 + z_4^T\dot{z}_4 \\ &\quad -\frac{1}{\eta_r}\mathrm{tr}(\tilde{W}_r^T\Gamma_r^{-1}\dot{\hat{W}}_r) - \frac{1}{\eta_{qs}}\mathrm{tr}(\tilde{W}_{qs}^T\Gamma_{qs}^{-1}\dot{\hat{W}}_{qs}) \\ &\quad -\frac{1}{\eta_{ds}}\mathrm{tr}(\tilde{W}_{ds}^T\Gamma_{ds}^{-1}\dot{\hat{W}}_{ds}) - \frac{1}{\eta_r}\Gamma_r^{-1}\tilde{\sigma}_r\dot{\hat{\sigma}}_r \\ &\quad -\frac{1}{\eta_{qs}}\Gamma_{qs}^{-1}\tilde{\sigma}_{qs}\dot{\hat{\sigma}}_{qs} - \frac{1}{\eta_{ds}}\Gamma_{ds}^{-1}\tilde{\sigma}_{ds}\dot{\hat{\sigma}}_{ds} \\ &= -k_1z_1^2 - k_2z_2^2 - k_3z_3^2 \\ &\quad +z_1(-u_r^{RC} + \sigma_r) + z_2(-u_{qs}^{RC} + \sigma_{qs}) \\ &\quad +z_3(-u_{ds}^{RC} + \sigma_{ds}) + z_1\tilde{W}_r^T\Xi_r + z_2\tilde{W}_{qs}^T\Xi_r + z_3\tilde{W}_{ds}^T\Xi_{ds} \\ &\quad -\frac{1}{\eta_r}\mathrm{tr}(\tilde{W}_r^T\Gamma_r^{-1}\dot{\hat{W}}_r) - \frac{1}{\eta_{qs}}\mathrm{tr}(\tilde{W}_{qs}^T\Gamma_{qs}^{-1}\dot{\hat{W}}_{qs}) \\ &\quad -\frac{1}{\eta_{ds}}\mathrm{tr}(\tilde{W}_{ds}^T\Gamma_{ds}^{-1}\dot{\hat{W}}_{ds}) - \frac{1}{\eta_r}\Gamma_r^{-1}\tilde{\sigma}_r\dot{\hat{\sigma}}_r \\ &\quad -\frac{1}{\eta_{qs}}\Gamma_{qs}^{-1}\tilde{\sigma}_{qs}\dot{\hat{\sigma}}_{qs} - \frac{1}{\eta_{ds}}\Gamma_{ds}^{-1}\tilde{\sigma}_{ds}\dot{\hat{\sigma}}_{ds}\end{aligned} \tag{68}$$

Compensating (55)-(63) into (68) will provide:

$$\begin{aligned}\dot{V}_a &= -k_1z_1^2 - k_2z_2^2 - k_3z_3^2 - k_4z_4^2 \\ &\quad +z_2(-u_r^{RC} + \sigma_r) + z_3(-u_{qs}^{RC} + \sigma_{qs}) + z_4(-u_{ds}^{RC} + \sigma_{ds}) \\ &\quad -\frac{1}{\eta_r}\Gamma_r^{-1}\tilde{\sigma}_r\dot{\hat{\sigma}}_r - \frac{1}{\eta_{qs}}\Gamma_{qs}^{-1}\tilde{\sigma}_{qs}\dot{\hat{\sigma}}_{qs} - \frac{1}{\eta_{ds}}\Gamma_{ds}^{-1}\tilde{\sigma}_{ds}\dot{\hat{\sigma}}_{ds} \\ &\leq -k_1z_1^2 - k_2z_2^2 - k_3z_3^2 - k_4z_4^2 \\ &\quad -|z_1|\,[u_r^{RC} - |\sigma_r|] - |z_2|\,[u_{qs}^{RC} - \left|\sigma_{qs}\right|] \\ &\quad -|z_3|\,[u_{ds}^{RC} - |\sigma_{ds}|] \\ &\leq -k_1z_1^2 - k_2z_2^2 - k_3z_3^2 - k_4z_4^2 \leq 0\end{aligned} \tag{69}$$

Since $\dot{V}_a(Z(t), \tilde{W}_k, \tilde{\sigma}_k(t))$ is a negative semidefinite function (i.e. $V_a(Z(t), \tilde{W}_k, \tilde{\sigma}_k(t)) \leq V_a(Z(0), \tilde{W}_k, \tilde{\sigma}_k(0))$, which denotes that $Z(t)$, $\tilde{W}_k$ and $\tilde{\sigma}_k(t)$ are limited functions. Determine the subsequent term as:

$$\Theta_a(t) \equiv k_1z_1^2 + k_2z_2^2 + k_3z_3^2 + k_4z_4^2 \leq -\dot{V}_a(Z(t), \tilde{W}_k, \tilde{\sigma}_k(t)) \tag{70}$$

where $Z = [z_1, z_2, z_3, z_4]$, $k = r, qs, ds$. Therefore:

$$\int_0^t \Theta_a(\tau)d\tau \leq V_a(Z(0), \tilde{W}_k, \tilde{\sigma}_k(0)) - V_a(Z(t), \tilde{W}_k, \tilde{\sigma}_k(t)) \tag{71}$$

Since $V_a(Z(0), \tilde{W}_k(0), \tilde{\sigma}_k(0)$ is a limited function while $V_a(Z(t), \tilde{W}_k(t), \tilde{\sigma}_k(t))$ is a limited and non-rising function, the next outcome can be acquired as:

$$\lim_{t\to\infty}\int_0^t \Theta_a(\tau)d\tau \leq \infty \tag{72}$$

Since $\dot{\Theta}_a(t)$ is a limited function, consequently $\Theta_a(t)$ is a symmetrical continuous function. By employing Barbalat's Lemma [52], it can be demonstrated that:

$$\lim_{t\to\infty}\Theta_a(t) = 0 \tag{73}$$

We can notice that as $t \to \infty$, the function $Z(t)$ will converge to zero. As a result, the stability of proposed RABC with RRBFNN-based uncertainty observer is guaranteed.

Remark 2: The lumped uncertainty terms σ_r, σ_{qs} and σ_{ds} comprise optimal parameters of the network, approximation errors, and higher order terms of Taylor series. Accordingly, a conservative control law with considerable limits is selected due to the unavailability of those terms in practical applications. In addition, the selection process of the upper limit of the uncertainty terms σ_r, σ_{qs} and σ_{ds} has a considerable influence on the performance of the control system. If the limits are chosen too large, the sign function of the controller may lead to a significant chattering incident in the control attempts. The unwanted chattering control attempts will trigger unsteady system dynamics. Contrarily, if the limits are chosen too small, the stability conditions may not be fulfilled. Thus, the HSPMSM drive system will be unstable. Hence, the adaptive bound estimation algorithms in (61)-(63) are used in this paper o simplify the adjustment of the limits in real time for the HSPMSM drive system based RRBFNN uncertainty observer.

Remark 3: According to Remark 1 and by comparison the RABC scheme with the backstepping control techniques in [19]–[26], the proposed strategy can resolve the problem of performance degradation by assessing the uncertainty terms in the dynamic model (9)-(15), Ω_r, Ω_{qs} and Ω_{ds}. In addition, the model uncertainties Ω_{qs} and Ω_{ds} of the drive system were not considered in [19]–[26]. Though, if the HSPMSM drive system parameters are perturbed (13)-(15), the control laws in [19]–[26] which consider only the mechanical uncertainty term (Ω_r) will lead to unstable drive system and the system performance may be degraded because the uncertainty terms Ω_{qs} and Ω_{ds} are not considered in the design step of the control method. The control laws in [19]–[26] only contains the neural network output. However, the control laws (43), (48) and (53) in this paper not only contains the RRBFNN output, which is utilized to estimate the parameter uncertainties, but also the developed robust controllers (58)-(60), which are intended to conform the values of lumped parameter uncertainties using the adaptive laws (61)-(63). Furthermore, the learning algorithms were only utilized to adjust the thresholds and weights of the neural network in [19]–[26] so as to give proper control performance. Nonetheless, in this paper, the learning algorithms (55)-(57), are utilized to online adapt the interior feedback, the center parameters, and the width parameters. Hence, to assure the the HSPMSM drive system stability in spite of the extrinsic load disturbance and dynamics of parameter uncertainties existed in (13)-(15), the RABC-based RRBFNN observer is suggested to compensate all these parameter uncertainties.

IV. VALIDATION RESULTS

In this section, the simulation and experimentation tests are performed to investigate the effectiveness of the proposed RABC scheme. The simulation tests are implemented through MATLAB/SIMULINK software according to the control schemes demonstrated in Figs. (1, 2). The schematic diagram of the experimental hardware setup is shown in Fig. 3.

A. EXPERIMENTAL SET-UP

The block diagram of the proposed control scheme with DSP-based controller for the high speed PMSM drive system is shown in Fig. 3. To implement the control operation, a DSP-based development controller board (dSPACE DS1102) with a TMS320C31 and TMS320P14 digital signal processors is utilized. The control board involves several input/output ports (PIO, ADC, DAC, and encoder) to acquire the measured signals and send the proper control actions. To enhance the precision of the measured feedback signals (position and speed), the encoder interface circuits uses a digital filter with frequency multiplied by four. The PWM signals of the inverter are generated based on a carrier frequency of 15 kHz which provides a sampling rate of 66.67μs. The position control loop utilizes a time interval of 1 ms. A six-IGBT switches were used to build the current-regulated PWM VSI. A 10000 pulses/revolution incremental optical encoder was applied to carry out the position acquisition. Consequently, a high precision measurement of the position/speed is resulted due to the high output frequency of the multiplier circuit (40000 pulses/revolution). Furthermore, the computed torque controller (CTC), the IBC and the proposed RABC schemes are implemented. Figure 4 shows the software flowcharts of the proposed RABC using RRBFNN.

The proposed real-time control algorithm implementation process consists of the main control program along

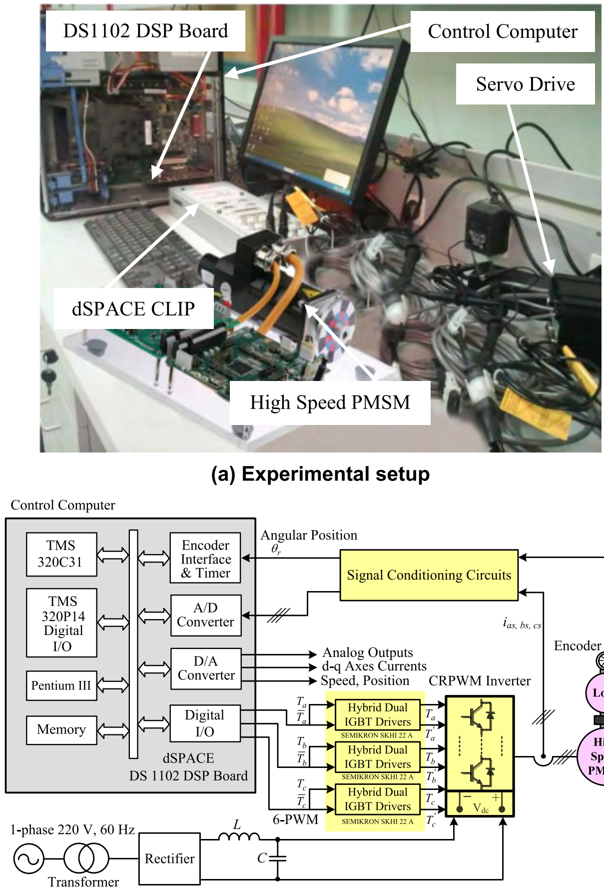

FIGURE 3. **The schematic diagram of the overall developed DSP-based high-speed drive system.**

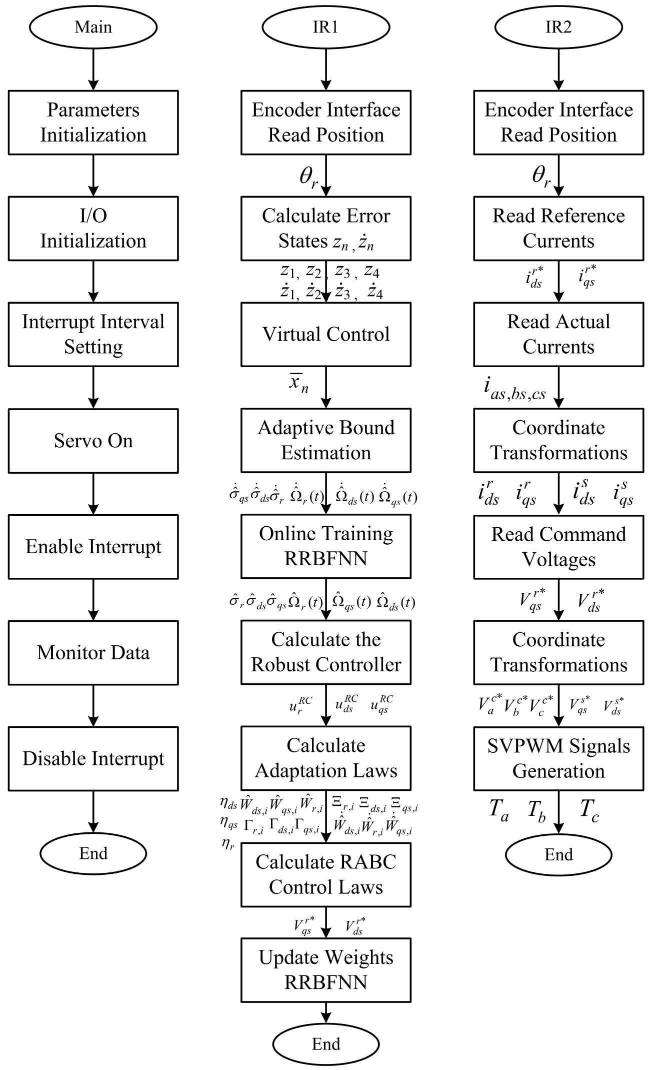

FIGURE 4. **Flowcharts of the RABC algorithm.**

with its subroutines. First, the initialization process of the input/output (I/O) and system parameters is set. After, the intervals for the two interrupt routines (IR1 and IR2) are set. Later, the counters of the encoder circuits are initialized by setting the servo drive. Once the interrupt is enabled, the main program is applied to observe the data of the control system. A sampling period of 1 ms is chosen to accomplish CPU calculations with high performance of the proposed RABC algorithm. The first interrupt subroutine (IR1) is utilized for the implementation of the control algorithms and the interface operation of the encoders. Initially, IR1 uses the encoders to examine the position of the HSPMSM. Next, IR1 with 1 ms sampling rate is utilized to calculate tracking error states (z_1, z_2, z_3 and z_4) and its derivatives ($\dot{z}_1$, $\dot{z}_2$, $\dot{z}_3$ and $\dot{z}_4$), the virtual control laws $\bar{x}_2$ and $\bar{x}_3$, real-time training of the RRBFNN and computation of the parameter uncertainties from the RRBFNN observer, calculation of the robust controllers, the adaptive control laws computation, the estimation of the adaptive limit algorithm, calculation of the RABC algorithm and updating the weights of the RRBFNN. Later, the IR2 with 0.2 ms sampling rate is utilized to collect the encoder data, perform the abc/d-q transformation, determine the d-q command currents, and perform d-q axis reference SVPWM voltages to generate the switching signals that control the inverter operation. Considering the stability needs and different operating condition, the parameters of the proposed RABC scheme are selected to accomplish the preferable tracking performance. An online parameter learning technique is used to retrieve the inaccurate initialization of system parameters. Hence, the adjustment operation of system parameters is regularly active for the whole running duration of experiments. Furthermore, the proposed RABC scheme parameters are: $\eta_{ds} = \eta_{qs} = 6.0$, $\eta_r = 3.0$, $k_1 = 9.5$, $k_2 = 3.5$, $k_3 = 7.5$ and $k_4 = 7.5$.

B. SIMULATION RESULTS

To investigate the feasibility of the proposed RABC scheme, the HSPMSM servo drive system is simulated and tested under various operating conditions. Subsequently, four different operating conditions of extrinsic load perturbations and parameter uncertainties (PUs) are studied to examine the robustness of the proposed controllers as follows:

Case 1: $1.0 \times (L_s/R_s)$, $1.0 \times (\beta_m/J_m)$, $1.00 \times \lambda_m$, $T_L = 0 - 0.5$ mN.m

Case 2: $0.5 \times (L_s/R_s)$, $1.5 \times (\beta_m/J_m)$, $0.85 \times \lambda_m$, $T_L = 0 - 0.5$ mN.m

Case 3: $1.5 \times (L_s/R_s)$, $2.5 \times (\beta_m/J_m)$, $1.25 \times \lambda_m$, $T_L = 0 - 0.5$ mN.m

Case 4: $1.5 \times (L_s/R_s)$, $5.0 \times (\beta_m/J_m)$, $1.25 \times \lambda_m$, $T_L = 0 - 0.5$ mN.m

For Case 1, we investigate the dynamic performance of the HSPMSM servo drive system under external loading command change 0-0.5 mN.m for the both IBC and RABC schemes while parameter ratios are maintained constant. Fig. 5 (a) shows the dynamic performance of the drive system with IBC scheme in terms of the reference and actual rotor positions, the position tracking error, the reference and actual rotor speeds, the speed tracking error, and $d-q$ axis currents, respectively. Moreover, the dynamic performance using the RABC scheme is investigated at the same operating conditions as depicted in Fig. 5 (b). At $t = 2.5$sec, the motor shaft is loaded by 0.5 mN.m then load is removed after at $t = 7.5$sec in order to check the disturbance rejection capabilities of both IBC and the proposed RABC. As seen from Fig. 4, the simulation results achieve good dynamic performances for both controllers under command change and load regulation. We can observe that the proposed RABC scheme provides better performance then IBC in load regulation and command tracking characteristics. Consequently, the results obtained from Fig. 4 show larger position and speed tracking errors with IBC scheme compared to the proposed RABC scheme with RRBFNN-based uncertainty observer. Furthermore, the results have demonstrated a substantial reduction of the utmost dip of both rotor position and speed with the proposed RABC scheme.

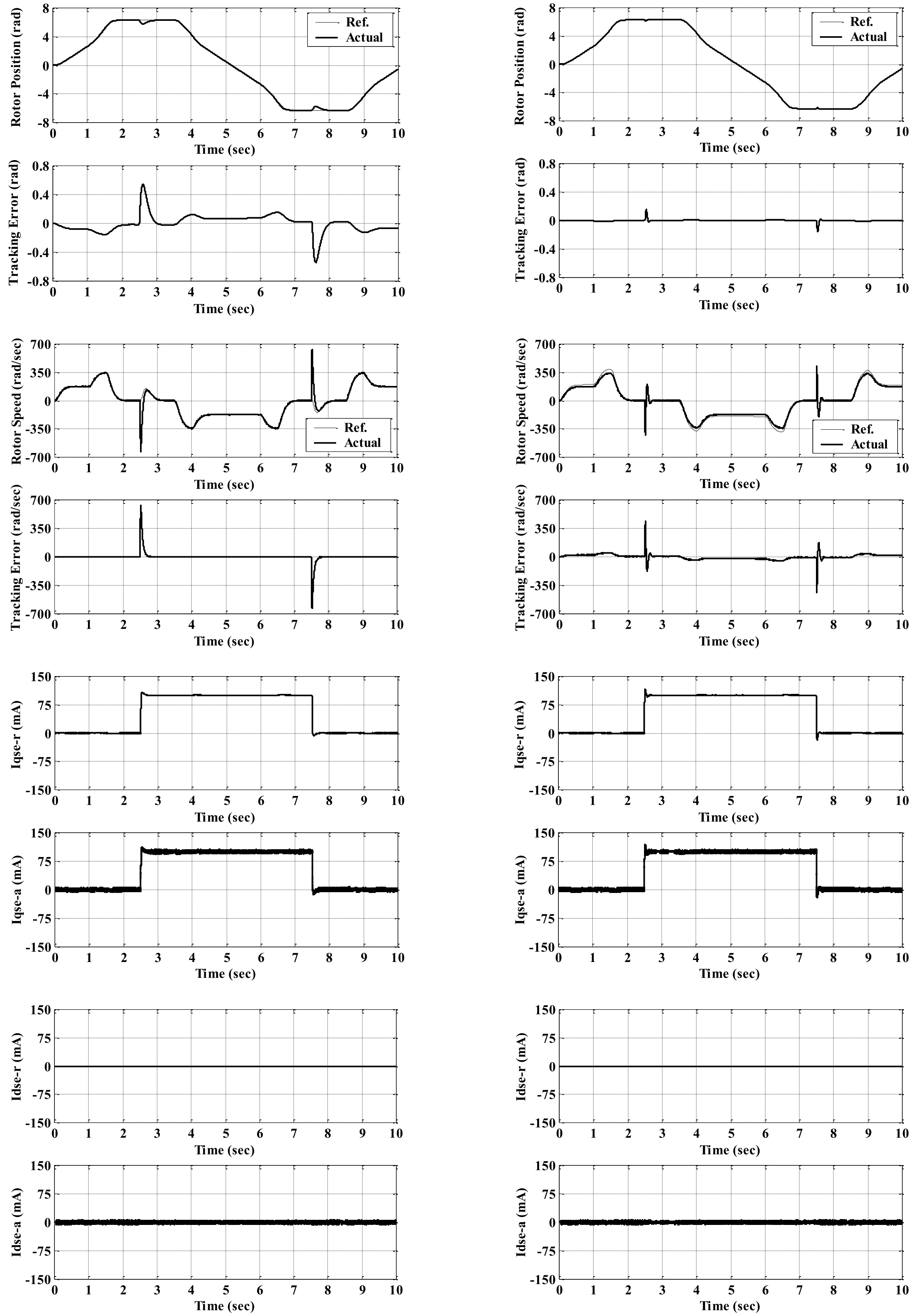

(a) Using IBC

(b) Using proposed RABC

FIGURE 5. Simulation results of the dynamic performance of the HSPMSM servo drive system with a reference position model of π rad and subsequent loading of 0.5 mN.m using: (a) the IBC and (b) the proposed RABC with RRBFNN-based uncertainty observer.

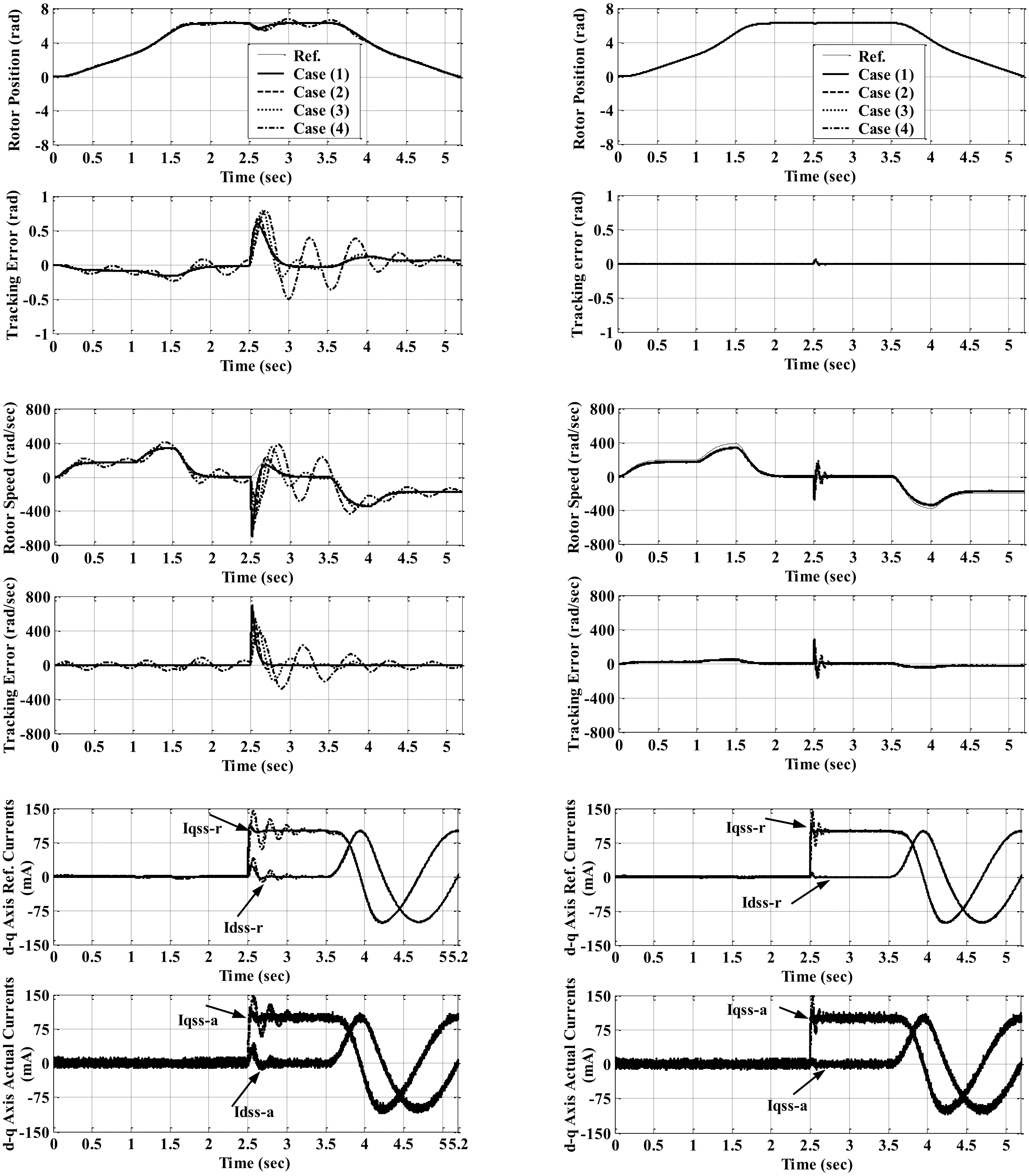

(a) Using IBC

(b) Using proposed RABC

FIGURE 6. **Simulation results for all different Cases (1-4) of the enlarged dynamic performance under PUs of the HSPMSM servo drive system with a reference position model of 2π rad and subsequent loading of 0.5 mN.m using: (a) the IBC and (b) the proposed RABC with RRBFNN-based uncertainty observer.**

In addition, the external load disturbance and PUs are further detailed investigated through four different cases (Case 1-4) to be compared in order to confirm the robustness capability of the proposed RABC scheme. Fig. 6 and 7 show the comparative dynamic performance at all Cases of PUs of the HSPMSM servo drive system for both the IBC and

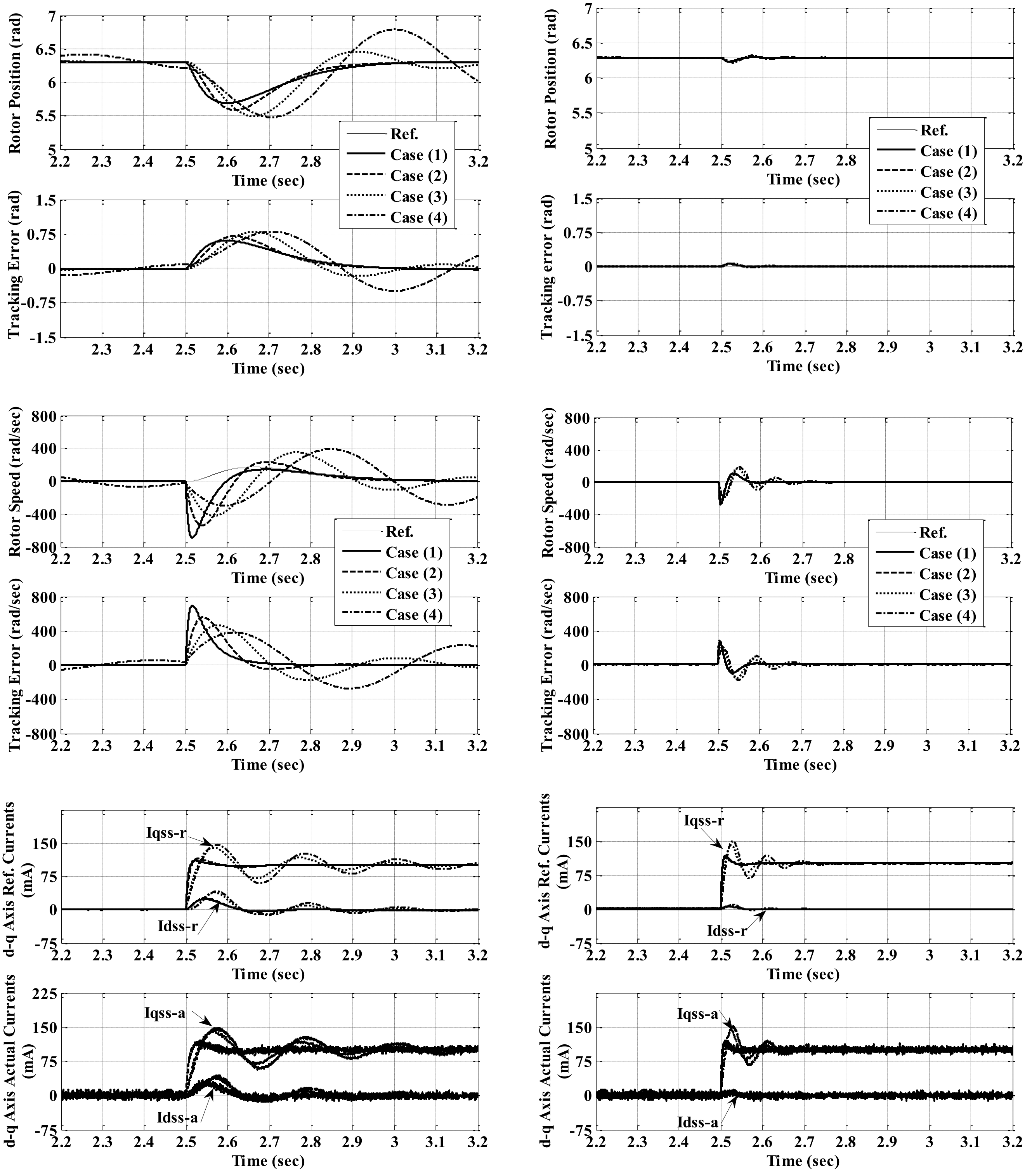

FIGURE 7. Simulation results for all different Cases (1-4) of the load regulation characteristics under PUs of the HSPMSM servo drive system using: (a) the IBC and (b) the proposed RABC with RRBFNN-based uncertainty observer.

the proposed RABC schemes. It is clearly noticed that the tracking errors quickly converge to zero which validate the robustness characteristics of the proposed RABC scheme under the incident of PUs. Thus, the tracking errors have been significantly reduced as well as load regulation capabilities have been verified compared to the IBC scheme. As a result,

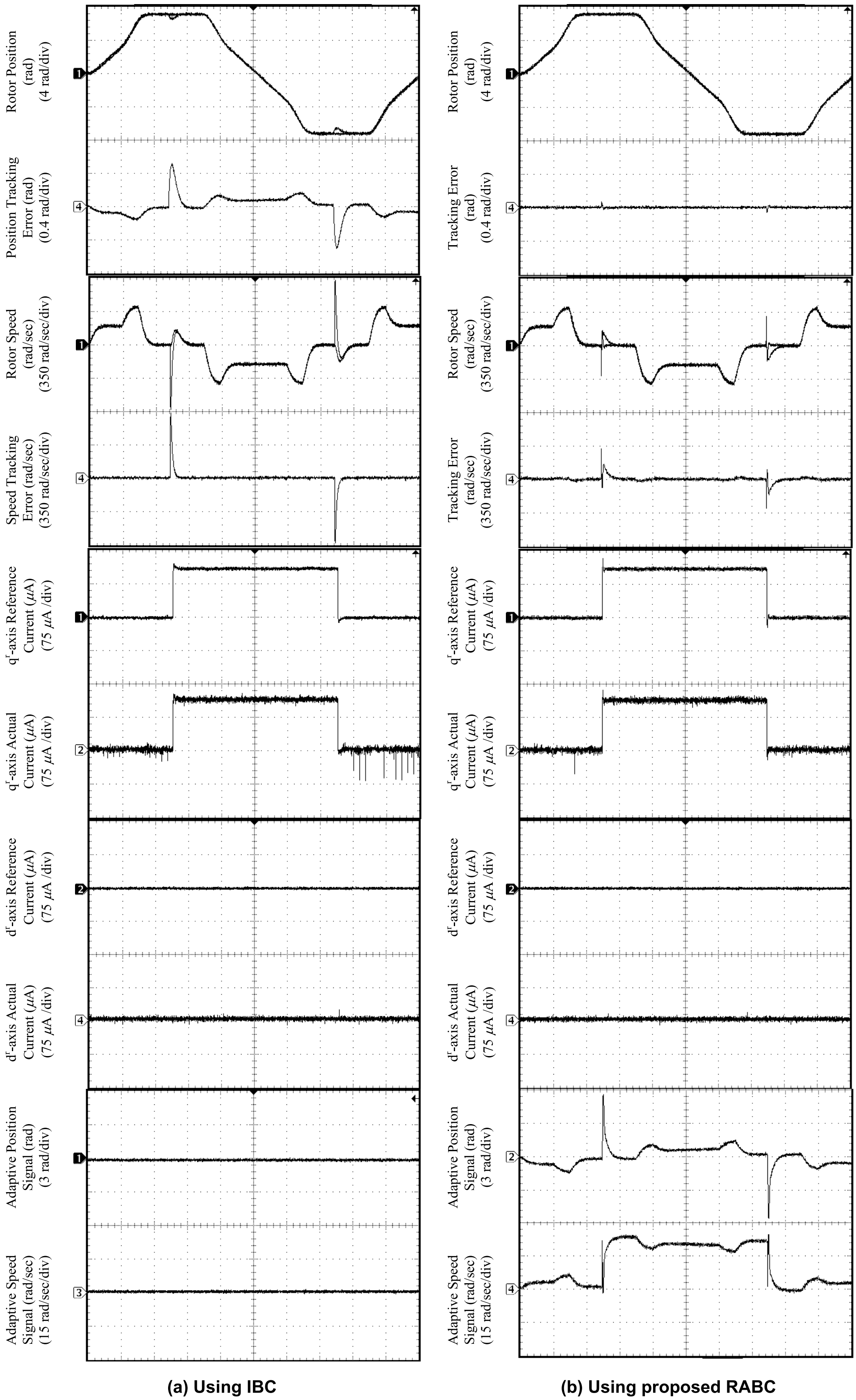

FIGURE 8. Experimental results of the dynamic performance of the HSPMSM servo drive system with a reference position model of 2π rad and subsequent loading of 0.5 mN.m using: (a) the IBC and (b) the proposed RABC with RRBFNN-based uncertainty observer.

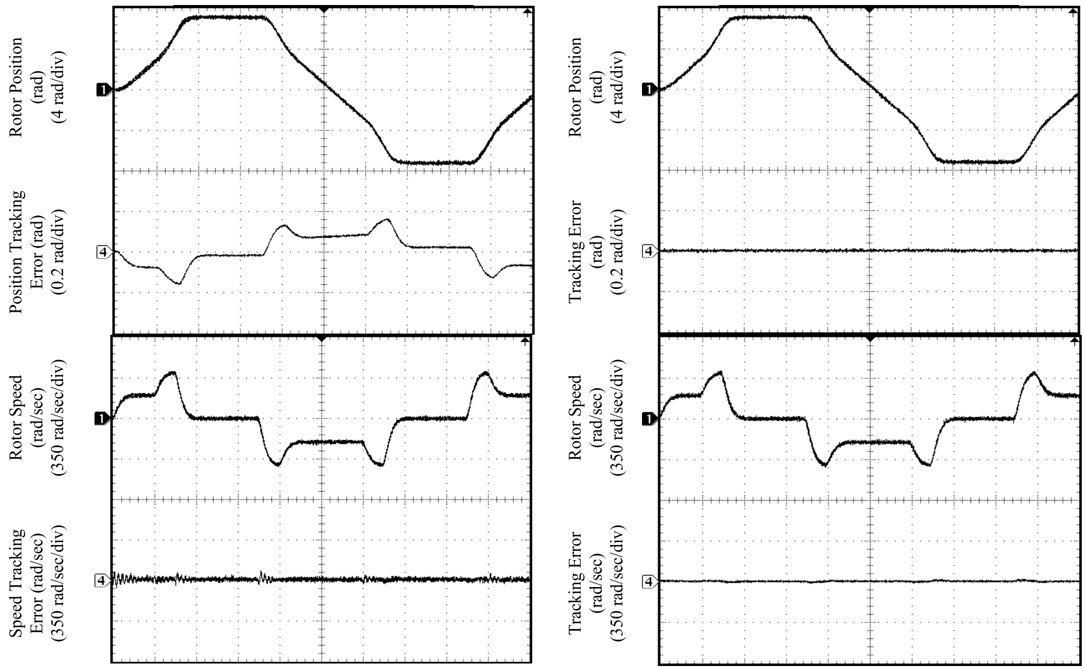

(a) Using IBC (b) Using proposed RABC

FIGURE 9. Experimental results of the dynamic performance of the HSPMSM servo drive system with a reference position model of 2π rad at no-load condition using: (a) IBC and (b) proposed RABC with RRBFNN-based uncertainty observer.

the designed RABC structure can provide preferable control response compared to the IBC structure. In addition, the proposed RABC scheme yields a faster response (within 0.2 sec) and higher precision than the IBC scheme for the reference model under load variations. On the other hand, the IBC under PUs has indolent recovery time (>2.5 sec). Eventually, for all cases of PUs, it can be confirmed that the proposed RABC scheme provides several advantages in terms of its tracking accuracy, robustness, as well as suitability with the HSPMSM control system

C. EXPERIMENTAL RESULTS

A hardware experimental prototype of the HSPMSM with the same simulation parameters was tested to validate the high performance of the developed RABC scheme compared to the IBC scheme. The laboratory tests were performed based on the control schemes presented in Figs. (1-4).

To further investigate the effectiveness of the developed control schemes for micro drive-based industrial applications, experimental test findings are presented. Fig. 8 shows comparative test results for the dynamic performance of the IBC versus the developed RABC under desired model command with subsequent applied loading condition of 0.5 mN.m. The dynamic responses of the IBC involving the reference and actual rotor positions, the position tracking error, the reference and actual rotor speeds, the speed tracking error, the $d - q$ axis currents, and adaptive position/speed signals are depicted in Fig. 8(a). Furthermore, the dynamic responses of the proposed RABC including same signals are shown in Fig. 8(b). In addition, the results have shown better disturbance rejection capability with the proposed RABC scheme compared to the IBC scheme. At full load condition, we can also notice that the proposed RABC with the RRBFNN-based uncertainty observer provides less maximum position tracking errors of ~0.15 rad while the IBC has higher error of ~0.6 rad. Obviously, the test results acquired in Fig. 8 show better dynamic response of the proposed RABC scheme accomplishing preferable load regulation and command tracking. Moreover, the drive system performance has been investigated for both IBC and RABC schemes at no-load condition as displayed in Fig. 9. It is clearly illustrated that the proposed RABC gives better regulation characteristics as well as significantly reduced position/speed tracking errors compared with the IBC. Subsequently, the proposed RABC scheme validates its superiority performance compared with the IBC. Undoubtedly, the RABC scheme with RRBFNN-based uncertainty observer has verified its preferable performance for the HSPMSM drive applications with greatly improved characteristics to a great extent. Consequently, it was proved that the developed RABC design accomplishes the precision demands, robustness, and suitability for high performance industrial drive applications.

D. EVALUATION AND COMPARISON OF CONTROL PERFORMANCE

To evaluate the performance of the servo drive system, we will use three tracking error indices (maximum, average, and standard deviation) [18], [40]. The control response can be readily compared utilizing (74)-(76) as follows:

$$TE_{\max} = \max_{k} \sqrt{T(k)^2} \tag{74}$$

$$TE_{mean} = \sum_{k=1}^{n} \frac{T(k)}{n} \tag{75}$$

$$TE_{sd} = \sqrt{\sum_{k=1}^{n} \frac{(T(k) - T_{mean})^2}{n}} \tag{76}$$

where TE_{max} is the maximum tracking error, TE_{mean} is the average tracking error, TE_{sd} is the standard deviation of the tracking error, $T(k) = [\theta_r^m(k) - \theta_r(k)]$.

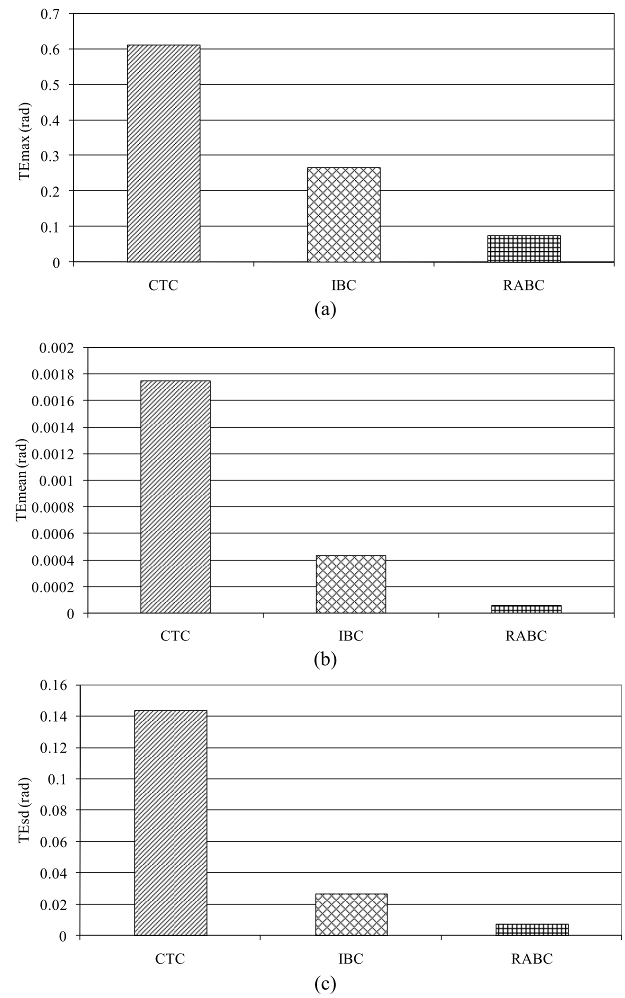

FIGURE 10. **Performance measures of CTC, IBC and proposed RABC schemes for HSPMSM servo drive system (experimentation): (a) TEmax, (b) TEmean, and (c) TEsd.**

The performance evaluation of the different position controllers schemes are depicted in Fig. 10. The various comparative performance average measures with respect to computed torque controller (CTC) show that the proposed RABC provides lower tracking errors by: 87.66% for maximum error, 96.48% for average error and 94.74% for standard deviation error. In regard to IBC compared to CTC, the averages of

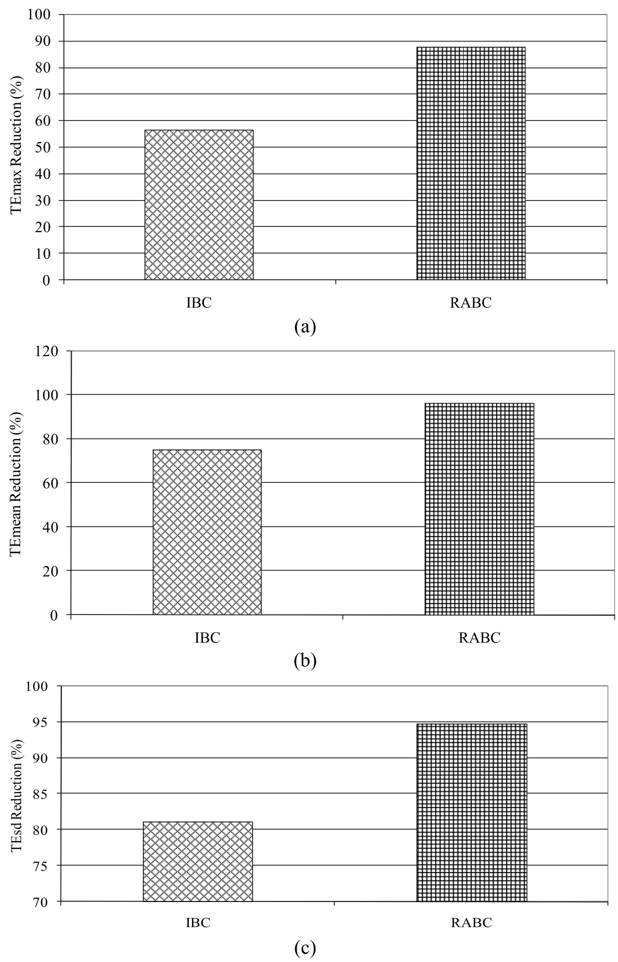

FIGURE 11. **Tracking errors reduction percentage using IBC and proposed RABC schemes for HSPMSM servo drive system (experimentation): (a) TEmax, (b) TEmean, and (c) TEsd.**

TABLE 2. **Performance evaluation of the HSPMSM servo drive system (experimentation).**

Controller Type	Tracking Errors (rad)		
	Maximum	Average	S.D.
CTC	0.6125	0.0017560	0.14370
IBC	0.2673	0.0004375	0.02682
RABC	0.0756	6.185e-005	0.00756

the maximum, average, standard deviation tracking errors are decreased by 56.36%, 75.10% and 81.13%, respectively. The percentage reductions of the tracking errors utilizing the IBC and the proposed RABC schemes compared to the CTC scheme are shown in Fig. 11. The comparative analysis of the control performance is illustrated in Table 2. Furthermore, Table 3 depicts the improvement in the tracking errors with IBC and proposed RABC in comparison to the CTC. It is apparent that the performance measures of the HSPMSM servo drive system are significantly enhanced with the proposed RABC scheme. Consequently, the developed RABC with RRBFNN-based uncertainty observer fulfills the high precision demands. Thus, the proposed scheme has verified

TABLE 3. Percentage reductionof tracking errors based on CTC (experimentation).

Controller Type	Tracking Errors Reduction (%)		
	Maximum	Average	S.D.
IBC	56.36	75.10	81.13
RABC	87.66	96.48	94.74

its superiority for the position/speed control of the HSPMSM servo drive systems for industrial applications.

V. CONCLUSION

In this paper, we proposed an RABC using RRBFNN uncertainty observer for HSPMSM adjustable speed drives to achieve high dynamic control performance in the existence of parameter uncertainties and extrinsic load perturbations. The RABC scheme encompasses an IBC, a RRBFNN uncertainty observer and a robust controller. First, the IBC is designed in the sense of Lyapunov stability theorem to stabilize the HSPMSM drive system and to satisfy multiple objectives of a stable rotor position to trace the desired trajectory. Though, certain information about the lumped parameter uncertainties are needed within the backstepping control law so that the system performance would not severely affected. Consequently, an RABC was developed to enhance the robustness of the HSPMSM drive system as a result of extrinsic load perturbations as well as parameter uncertainties. Thus, an online adaptive observer based on RRBFNN was incorporated to estimate the nonlinear parameter uncertainties. Moreover, the robust controller was developed to retrieve the remaining of the RRBFNN estimate errors. To assure the stability of the developed RABC, the Lyapunov stability analysis has been used to derive the online adaptive control laws. Experimental tests of the HSPMSM drive system were performed to confirm the validation of the designed RABC scheme. The dynamic performance of the HSPMSM drive system has been studied under wide range of operating conditions. The test results assure an improved dynamic response and robust control performance of the developed RABC regardless the parameter changes and load disturbances. In conclusion, the main contributions of this paper can be summarized as: a novel RABC was successfully developed, implemented, and applied for the HSPMSM drive system to achieve robust control performance considering load disturbances and parameters uncertainties; a new model of RRBFNN-based online uncertainty observer was effectively designed to conform the nonlinear uncertainties.

APPENDIX

A. ON-LINE LEARNING ALGORITHM OF THE RRBFNN

To describe the on-line parameter learning algorithm, first the energy function E_n is defined as

$$E_n = (1/2)(x_n^d - x_n)^2 = (1/2)(z_n)^2 \tag{A.1}$$

where $x_n^d(t)$ is the reference command, $x_n(t)$ is the actual state and z_n is the error signal between the reference command and the actual state; $n = 1, 2, \cdots, 4$. The learning algorithm based on the BP is described as follows.

Layer 3: In the output layer, the error term to be propagated is calculated as:

$$\begin{aligned}\delta_o^3(N+1) &= -\frac{\partial E_n}{\partial net_o^3}(N+1)\\ &= \left[-\frac{\partial E_n}{\partial z_n^n}\frac{\partial z_n^n}{\partial y_o^3}\right] = \left[-\frac{\partial E_n}{\partial z_n^n}\frac{\partial z_n^n}{\partial u}\frac{\partial u}{\partial y_o^3}\right]\end{aligned} \tag{A.2}$$

The weight is updated by the amount:

$$\begin{aligned}&\Delta W_j(N+1)\\ &\quad = -\eta_W \frac{\partial E_n}{\partial W_j}(N+1)\\ &\quad = \left[-\eta_W \frac{\partial E_n}{\partial y_o^3}\frac{\partial y_o^3}{\partial net_o^3}\frac{\partial net_o^3}{\partial W_j}\right] = \eta_W \delta_o^3(N+1)\Phi_j^2\end{aligned} \tag{A.3}$$

$$\begin{aligned}&\Delta W_o(N+1)\\ &\quad = -\eta_o \frac{\partial E_n}{\partial W_o}(N+1)\\ &\quad = \left[-\eta_o \frac{\partial E_n}{\partial y_o^3}\frac{\partial y_o^3}{\partial net_o^3}\frac{\partial net_o^3}{\partial W_o}\right] = \eta_o \delta_o^3(N+1)y_o^l\end{aligned} \tag{A.4}$$

$$\begin{aligned}&\Delta \beta_o^l(N+1)\\ &\quad = -\eta_\beta \frac{\partial E_n}{\partial \beta_o^l}(N+1)\\ &\quad = \left[-\eta_o \frac{\partial E_n}{\partial y_o^3}\frac{\partial y_o^3}{\partial net_o^3}\frac{\partial net_o^3}{\partial \beta_o^l}\right] = \eta_\beta \delta_o^3(N+1)y_o^l\end{aligned} \tag{A.5}$$

where η_W, η_o and η_β are the learning rate parameter of the connecting weights between the hidden layer and the output layer of the RRBFN. The weights of the output layer are updated according to the following equations.

$$W_j(N+1) = W_j(N) + \Delta W_j(N+1) \tag{A.6}$$

$$W_o(N+1) = W_o(N) + \Delta W_o(N+1) \tag{A.7}$$

$$\beta_o^l(N+1) = \beta_o^l(N) + \Delta\beta_o^l(N+1) \tag{A.8}$$

Layer 2: In the hidden layer, the error term is calculated as:

$$\begin{aligned}\delta_j^2 &= -\frac{\partial E_n}{\partial net_j^2} = -\frac{\partial E_n}{\partial \tilde{A}_i^j} = \left(-\frac{\partial E_n}{\partial y_o^3}\frac{\partial y_o^3}{\partial net_o^3}\frac{\partial net_o^3}{\partial y_j^2}\frac{\partial y_j^2}{\partial \tilde{A}_i^j}\right)\\ &= \sum_j W_j\Phi_j\end{aligned} \tag{A.9}$$

The update laws of the μ_i^j and the σ_i^j are given by:

$$\begin{aligned}\Delta\mu_i^j(N+1) &= -\eta_\mu \frac{\partial E_n}{\partial \mu_i^j}(N+1) = \left[-\eta_\mu \frac{\partial E_n}{\partial\partial\tilde{A}_i^j}\frac{\partial\partial\tilde{A}_i^j}{\partial\mu_i^j}\right]\\ &= \eta_\mu \delta_j^2(N+1)\cdot\tilde{A}_i^j(\Phi_i^j)\\ &\quad \cdot\left((\Phi_j-\mu_j)^T\sigma_j(\Phi_j-\mu_j)\right)(N-1)\\ &\quad \times\left(\frac{\partial\Phi_i^j}{\partial\mu_i^j}(N)-1\right)\end{aligned} \tag{A.10}$$

$$\frac{\partial \Phi_i^j}{\partial \mu_i^j}(N) = \zeta_i^j(N-1)\alpha_i^j(N) \cdot \left((\Phi_j - \mu_j)^T \sigma_j(\Phi_j - \mu_j)\right)(N-1) \times \left(\frac{\partial \Phi_i^j}{\partial \mu_i^j}(N) - 1\right) \tag{A.11}$$

$$\Delta\sigma_i^j(N+1) = -\eta_\sigma \frac{\partial E_n}{\partial \sigma_i^j}(N+1) = \left[-\eta_\sigma \frac{\partial E_n}{\partial \tilde{A}_i^j}\frac{\partial \tilde{A}_i^j}{\partial \sigma_i^j}\right] = \eta_\sigma \delta_j^2(N+1)\cdot \tilde{A}_i^j(\Phi_i^j) \cdot \left((\Phi_j - \mu_j)^T \sigma_j(\Phi_j - \mu_j)\right)(N-1) \tag{A.12}$$

$$\frac{\partial \Phi_i^j}{\partial \sigma_i^j}(N) = \zeta_i^j(N-1)\alpha_i^j(N) \cdot \left((\Phi_j - \mu_j)^T \sigma_j(\Phi_j - \mu_j)\right)(N-1) \tag{A.13}$$

The update weight of the feedback, α_i^j, is:

$$\Delta\alpha_i^j(N+1) = -\eta_\alpha \frac{\partial E_n}{\partial \alpha_i^j}(N+1) = \left[-\eta_\alpha \frac{\partial E_n}{\partial \tilde{A}_i^j}\frac{\partial \tilde{A}_i^j}{\partial \alpha_i^j}\right] = \eta_\alpha \delta_j^2(N+1)\cdot \tilde{A}_i^j(\Phi_i^j) \cdot \left((\Phi_j - \mu_j)^T \sigma_j(\Phi_j - \mu_j)\right)(N)\left(\frac{\partial \Phi_i^j}{\partial \alpha_i^j}(N)\right) \tag{A.14}$$

$$\frac{\partial \Phi_i^j}{\partial \alpha_i^j}(N) = \zeta_i^j(N-1)\alpha_i^j(N) \cdot \left((\Phi_j - \mu_j)^T \sigma_j(\Phi_j - \mu_j)\right)(N-1)\left(\frac{\partial \Phi_i^j}{\partial \alpha_i^j}(N) - 1\right) + \zeta_i^j(N-1) \tag{A.15}$$

where η_μ and η_σ and η_α are the learning rate parameters of the mean, standard deviation and the self-feedback loop, respectively. Moreover, they can be updated as follows:

$$\mu_j^i(N+1) = \mu_j^i(N) + \Delta\mu_j^i(N+1) \tag{A.16}$$

$$\sigma_j^i(N+1) = \sigma_j^i(N) + \Delta\sigma_j^i(N+1) \tag{A.17}$$

$$\alpha_j^i(N+1) = \alpha_j^i(N) + \Delta\alpha_j^i(N+1) \tag{A.18}$$

The exact calculation of the Jacobian of the HSPMSM drive system $(\partial x_n/\partial y_o^3)$ in (A.2), cannot be easily determined and need heavy computation due to the uncertainties of the servo drive system dynamic, such as parameter variations and external load disturbances. To overcome this problem and to increase the online learning speed of the network parameters, the sensitivity of the system in (A.2) can be approximated by its sign function [27], [49], [50] as:

$$\frac{\partial x_n}{\partial y_o^3} \cong \operatorname{sgn}\left(\frac{x_n(N) - x_n(N-1)}{y_o^3(N) - y_o^3(N-1)}\right) \tag{A.19}$$

where sgn(·) is the sign function.

B. CONVERGENCE ANALYSES OF THE RRBFNN

Consider the energy function in (A.1) as a discrete-type Lyapunov function and the change in the Lyapunov function can be written as:

$$\begin{aligned}E_n(N+1) &= E_n(N) + \Delta E_n(N) \\ &\approx E_n(N) + \sum_{j=1}^{n_y}\sum_{o=1}^{n_o}\left[\frac{\partial E_n(N)}{\partial W_j}\Delta W_j\right] + \sum_{l=1}^{n_y}\sum_{o=1}^{n_o}\left[\frac{\partial E_n(N)}{\partial W_o}\Delta W_o\right] + \sum_{l=1}^{n_y}\sum_{o=1}^{n_o}\left[\frac{\partial E_n(N)}{\partial \beta_o^l}\Delta \beta_o^l\right] \\ &\quad + \sum_{i=1}^{n_i}\sum_{j=1}^{n_j}\left[\frac{\partial E_n(N)}{\partial \mu_i^j}\Delta\mu_i^j + \frac{\partial E_n(N)}{\partial \sigma_i^j}\Delta\sigma_i^j + \frac{\partial E_n(N)}{\partial \alpha_i^j}\Delta\alpha_i^j\right]\end{aligned} \tag{B.1}$$

$$\begin{aligned}E_n(N+1) &= \frac{1}{6}E_n(N) - \eta_W \sum_{j=1}^{n_y}\sum_{o=1}^{n_o}\left(\frac{\partial E_n(N)}{\partial y_o^3}\frac{\partial y_o^3}{\partial W_j}\right)^2 + \frac{1}{6}E_n(N) - \eta_o \sum_{l=1}^{n_y}\sum_{o=1}^{n_o}\left(\frac{\partial E_n(N)}{\partial y_o^3}\frac{\partial y_o^3}{\partial W_o}\right)^2 \\ &\quad + \frac{1}{6}E_n(N) - \eta_\beta \sum_{l=1}^{n_y}\sum_{o=1}^{n_o}\left(\frac{\partial E_n(N)}{\partial y_o^3}\frac{\partial y_o^3}{\partial \beta_o^l}\right)^2 + \frac{1}{6}E_n(N) - \eta_\mu \sum_{i=1}^{n_i}\sum_{j=1}^{n_j}\sum_{o=1}^{n_o}\left(\frac{\partial E_n(N)}{\partial x_n^i}\frac{\partial x_n^i}{\partial y_o^3}\frac{\partial y_o^3}{\partial \mu_i^j}\right)^2 \\ &\quad + \frac{1}{6}E_n(N) - \eta_\sigma \sum_{i=1}^{n_i}\sum_{j=1}^{n_j}\sum_{o=1}^{n_o}\left(\frac{\partial E_n(N)}{\partial x_n^i}\frac{\partial x_n^i}{\partial y_o^3}\frac{\partial y_o^3}{\partial \sigma_i^j}\right)^2 + \frac{1}{6}E_n(N) - \eta_\alpha \sum_{i=1}^{n_i}\sum_{j=1}^{n_j}\sum_{o=1}^{n_o}\left(\frac{\partial E_n(N)}{\partial x_n^i}\frac{\partial x_n^i}{\partial y_o^3}\frac{\partial y_o^3}{\partial \alpha_i^j}\right)^2\end{aligned} \tag{B.2}$$

where ΔW_j, ΔW_o, $\Delta\mu_j^i$, $\Delta\sigma_j^i$, $\Delta\beta_o^l$ and $\Delta\alpha_j^i$ represent the weight change in the output layer, the mean and standard deviation in the Gaussian function and the weight change in the self-feedback loops, respectively. If the learning rate parameters of the RRBFNN are designated as

$$\eta_W = \frac{E_n(N)}{6\left[\sum_{j=1}^{n_y}\sum_{o=1}^{n_o}\left(\frac{\partial E_n(N)}{\partial y_o^3}\frac{\partial y_o^3}{\partial W_j}\right)^2 + \nu\right]} \tag{B.3}$$

$$\eta_o = \frac{E_n(N)}{6\left[\sum_{j=1}^{n_y}\sum_{o=1}^{n_o}\left(\frac{\partial E_n(N)}{\partial y_o^3}\frac{\partial y_o^3}{\partial W_o}\right)^2 + \nu\right]} \tag{B.4}$$

$$\eta_\beta = \frac{E_n(N)}{6\left[\sum_{l=1}^{n_y}\sum_{o=1}^{n_o}\left(\frac{\partial E_n(N)}{\partial y_o^3}\frac{\partial y_o^3}{\partial \beta_o^l}\right)^2 + \nu\right]} \tag{B.5}$$

$$\eta_\mu = \frac{E_n(N)}{6\left[\sum_{i=1}^{n_i}\sum_{j=1}^{n_j}\sum_{o=1}^{n_o}\left(\frac{\partial E_n(N)}{\partial x_n^i}\frac{\partial x_n^i}{\partial y_o^3}\frac{\partial y_o^3}{\partial \mu_i^j}\right)^2+\nu\right]} \tag{B.6}$$

$$\eta_\sigma = \frac{E_n(N)}{6\left[\sum_{i=1}^{n_i}\sum_{j=1}^{n_j}\sum_{o=1}^{n_o}\left(\frac{\partial E_n(N)}{\partial x_n^i}\frac{\partial x_n^i}{\partial y_o^3}\frac{\partial y_o^3}{\partial \sigma_i^j}\right)^2+\nu\right]} \tag{B.7}$$

$$\eta_\alpha = \frac{E_n(N)}{6\left[\sum_{i=1}^{n_i}\sum_{j=1}^{n_j}\sum_{o=1}^{n_o}\left(\frac{\partial E_n(N)}{\partial x_n^i}\frac{\partial x_n^i}{\partial y_o^3}\frac{\partial y_o^3}{\partial \alpha_i^j}\right)^2+\nu\right]} \tag{B.8}$$

where ν is a positive constant, then (B.2) can be rewritten as

$$\begin{aligned}
E_n(N+1) &\approx \nu(\eta_W+\eta_o+\eta_\beta+\eta_\mu+\eta_\sigma+\eta_\alpha)\\
&= \frac{\nu E_n(N)}{6\left[\sum_{j=1}^{n_y}\sum_{o=1}^{n_o}\left(\frac{\partial E_n(N)}{\partial y_o^3}\frac{\partial y_o^3}{\partial W_j}\right)^2+\nu\right]}\\
&\quad+\frac{\nu E_n(N)}{6\left[\sum_{j=1}^{n_y}\sum_{o=1}^{n_o}\left(\frac{\partial E_n(N)}{\partial y_o^3}\frac{\partial y_o^3}{\partial W_o}\right)^2+\nu\right]}\\
&\quad+\frac{\nu E_n(N)}{6\left[\sum_{l=1}^{n_y}\sum_{o=1}^{n_o}\left(\frac{\partial E_n(N)}{\partial y_o^3}\frac{\partial y_o^3}{\partial \beta_o^l}\right)^2+\nu\right]}\\
&\quad+\frac{\nu E_n(N)}{6\left[\sum_{i=1}^{n_i}\sum_{j=1}^{n_j}\sum_{o=1}^{n_o}\left(\frac{\partial E_n(N)}{\partial x_n^i}\frac{\partial x_n^i}{\partial y_o^3}\frac{\partial y_o^3}{\partial \mu_i^j}\right)^2+\nu\right]}\\
&\quad+\frac{\nu E_n(N)}{6\left[\sum_{i=1}^{n_i}\sum_{j=1}^{n_j}\sum_{o=1}^{n_o}\left(\frac{\partial E_n(N)}{\partial x_n^i}\frac{\partial x_n^i}{\partial y_o^3}\frac{\partial y_o^3}{\partial \sigma_i^j}\right)^2+\nu\right]}\\
&\quad+\frac{\nu E_n(N)}{6\left[\sum_{i=1}^{n_i}\sum_{j=1}^{n_j}\sum_{o=1}^{n_o}\left(\frac{\partial E_n(N)}{\partial x_n^i}\frac{\partial x_n^i}{\partial y_o^3}\frac{\partial y_o^3}{\partial \alpha_i^j}\right)^2+\nu\right]}\\
&< \frac{E_n(N)}{6}+\frac{E_n(N)}{6}+\frac{E_n(N)}{6}+\frac{E_n(N)}{6}\\
&\quad+\frac{E_n(N)}{6}+\frac{E_n(N)}{6}=E_n(N)
\end{aligned} \tag{B.9}$$

According to (A.1) and (B.9), the convergent ability of the RRBFNN can be guaranteed.

REFERENCES

[1] K. Hameyer and R. Belmans, "Design of very small electromagnetic and electrostatic micro motors," *IEEE Trans. Energy Convers.*, vol. 14, no. 4, pp. 1241–1246, Dec. 1999.

[2] P. L. Chapman and P. T. Krein, "Smaller is better? [micromotors and electric drives]," *IEEE Ind. Appl. Mag.*, vol. 9, no. 1, pp. 62–67, Jan. 2003.

[3] D. P. Arnold and N. Wang, "Permanent magnets for MEMS," *J. Microelectromech. Syst.*, vol. 18, no. 6, pp. 1255–1266, Dec. 2009.

[4] H. Ishihara, F. Arai, and T. Fukuda, "Micro mechatronics and micro actuators," *IEEE/ASME Trans. Mechatronics*, vol. 1, no. 1, pp. 68–79, Mar. 1996.

[5] T. C. Neugebauer, D. J. Perreault, J. H. Lang, and C. Livermore, "A six-phase multilevel inverter for MEMS electrostatic induction micromotors," *IEEE Trans. Circuits Syst. II, Exp. Briefs*, vol. 51, no. 2, pp. 49–56, Feb. 2004.

[6] J. Zhang and M. Schroff, "High-performance micromotor control systems," *IEEE IECON*, Nov. 2003, pp. 347–352.

[7] J. Zhang and Q. Jiang, "Sensorless commutation of micro PMSMs for high-performance high-speed applications," in *Proc. IEEE ICEMS*, Sep. 2005, pp. 1795–1800.

[8] Y. H. Chang, T. H. Liu, and C. C. Wu, "Design and implementation of an H_∞ controller for a micropermanent-magnet synchronous motor position control system," *IET Electr. Power Appl.*, vol. 2, no. 1, pp. 8–18, 2008.

[9] Y.-H. Chang, T.-H. Liu, and C.-C. Wu, "Novel adjustable micropermanent-magnet synchronous motor control system without using a rotor-position/speed sensor," *IEE Proc.-Electr. Power Appl.*, vol. 153, no. 3, pp. 429–438, 2006.

[10] Y.-H. Chang, T.-H. Liu, and D.-F. Chen, "Design and implementation of a robust controller for a micro permanent magnet synchronous speed control systems," in *Proc. IEEE ICICIC*, Sep. 2007, p. 99.

[11] S. E. Lysheski, "Mini- and microscale closed-loop servodrives with brushless minimotors and ICs monolithic amplifiers/controllers," in *Proc. IEEE CDC*, Dec. 2002, pp. 3670–3674.

[12] A. Purushotham, S. L. Garverick, C. Edwards, and M. L. Nagy, "A closed-loop micromotor control system," in *Proc. IEEE ISCAS*, May 1996, pp. 209–212.

[13] F. F. M. El-Sousy and S. A. Al-Kharj, "Intelligent hybrid controller for identification and control of micro permanent-magnet synchronous motor servo drive system using Petri recurrent-fuzzy-neural-network," *WSEAS Trans. Syst. Control*, vol. 9, pp. 336–355, Jul. 2014.

[14] T.-Y. Chang, T.-H. Liu, and T.-T. Chen, "Design and implementation of an adaptive inverse controller for a micro-permanent magnet synchronous motor control system," *IET Electr. Power Appl.*, vol. 3, no. 5, pp. 471–481, 2009.

[15] T.-Y. Chou, T.-H. Liu, and T.-T. Cheng, "Sensorless micro-permanent magnet synchronous motor control system with a wide adjustable speed range," *IET Electr. Power Appl.*, vol. 6, no. 2, pp. 62–72, 2012.

[16] T. Y. Chou and T. H. Liu, "Implementation of a motion control system using micro-permanent magnet synchronous motors," *IET Electr. Power Appl.*, vol. 6, no. 6, pp. 362–374, Jul. 2012.

[17] W.-C. Chi and M.-Y. Cheng, "Implementation of a sliding-mode-based position sensorless drive for high-speed micro permanent-magnet synchronous motors," *ISA Trans.*, vol. 53, no. 2, pp. 444–453, 2014.

[18] F. F. M. El-Sousy and K. A. Abuhasel, "Nonlinear adaptive backstepping control-based dynamic recurrent RBFN uncertainty observer for high-speed micro permanent-magnet synchronous motor drive system," in *Proc. IEEE Energy Convers. Congr. Expo.*, Portland, OR, USA, Sep. 2018, pp. 1696–1703.

[19] Y. Li, S. Qiang, X. Zhuang, and O. Kaynak, "Robust and adaptive backstepping control for nonlinear systems using RBF neural networks," *IEEE Trans. Neural Netw.*, vol. 15, no. 3, pp. 693–701, May 2004.

[20] T. Zhang, S. S. Ge, and C. C. Hang, "Adaptive neural network control for strict-feedback nonlinear systems using backstepping design," *Automatica*, vol. 36, no. 12, pp. 1835–1846, 2000.

[21] J. Y. Choi and J. A. Farrell, "Adaptive observer backstepping control using neural networks," *IEEE Trans. Neural Netw.*, vol. 12, no. 5, pp. 1103–1112, Sep. 2001.

[22] O. Kuljaca, N. Swamy, F. L. Lewis, and C. M. Kwan, "Design and implementation of industrial neural network controller using backstepping," *IEEE Trans. Ind. Electron.*, vol. 50, no. 1, pp. 193–201, Feb. 2003.

[23] Y. Tan, J. Chang, and H. Tan, "Adaptive backstepping control and friction compensation for AC servo with inertia and load uncertainties," *IEEE Trans. Ind. Electron.*, vol. 50, no. 5, pp. 944–952, Oct. 2003.

[24] C.-M. Lin and C.-F. Hsu, "Recurrent-neural-network-based adaptive-backstepping control for induction servomotors," *IEEE Trans. Ind. Electron.*, vol. 52, no. 6, pp. 1677–1684, Dec. 2005.

[25] F. J. Lin, P. H. Shieh, and P. H. Chou, "Robust adaptive backstepping motion control of linear ultrasonic motors using fuzzy neural network," *IEEE Trans. Fuzzy Syst.*, vol. 16, no. 3, pp. 676–692, Jun. 2008.

[26] C. M. Kwan and F. L. Lewis, "Robust backstepping control of induction motors using neural networks," *IEEE Trans. Neural Netw.*, vol. 11, no. 5, pp. 1178–1187, Sep. 2000.

[27] C.-H. Lee and C.-C. Teng, "Identification and control of dynamic systems using recurrent fuzzy neural networks," *IEEE Trans. Fuzzy Syst.*, vol. 8, no. 4, pp. 349–366, Aug. 2000.

[28] W.-Y. Wang, T.-G. Leu, and C.-C. Hsu, "Robust adaptive fuzzy-neural control of nonlinear dynamical systems using generalized projection update law and variable structure controller," *IEEE Trans. Syst., Man, Cybern. B, Cybern.*, vol. 31, no. 1, pp. 140–147, Feb. 2001.

[29] C.-H. Wang, H.-L. Liu, and T.-C. Lin, "Direct adaptive fuzzy-neural control with state observer and supervisory controller for unknown nonlinear dynamical systems," *IEEE Trans. Fuzzy Syst.*, vol. 10, no. 1, pp. 39–49, Feb. 2002.

[30] O. Castillo and P. Melin, "Intelligent adaptive model-based control of robotic dynamic systems with a hybrid fuzzy-neural approach," *Appl. Soft Comput.*, vol. 3, no. 4, pp. 363–378, Dec. 2003.

[31] C.-J. Lin and C.-H. Chen, "Nonlinear system control using self-evolving neural fuzzy inference networks with reinforcement evolutionary learning," *Appl. Soft Comput.*, vol. 11, no. 8, pp. 5463–5476, 2011.

[32] C.-F. Hsu and K.-H. Cheng, "Recurrent Fuzzy-Neural approach for nonlinear control using dynamic structure learning scheme," *Neurocomputing*, vol. 71, nos. 16–18, pp. 3447–3459, 2008.

[33] H.-C. Lu, M.-H. Chang, and C.-H. Tsai, "Adaptive self-constructing fuzzy neural network controller for hardware implementation of an inverted pendulum system," *Appl. Soft Comput.*, vol. 11, no. 5, pp. 3962–3975, Jul. 2011.

[34] Y.-S. Lu and J.-S. Chen, "A self-organizing fuzzy sliding-mode controller design for a class of nonlinear servo systems," *IEEE Trans. Ind. Electron.*, vol. 41, no. 5, pp. 492–502, Oct. 1994.

[35] F. F. M. El-Sousy, "Adaptive hybrid control system using a recurrent rbfn-based self-evolving fuzzy-neural-network for PMSM servo drives," *Appl. Soft Comput.*, vol. 21, no. 8, pp. 509–532, Aug. 2014.

[36] J.-S. R. Jang and C.-T. Sun, "Functional equivalence between radial basis function networks and fuzzy inference systems," *IEEE Trans. Neural Netw.*, vol. 4, no. 1, pp. 156–159, Jan. 1993.

[37] S. Seshagiri and H. K. Khalil, "Output feedback control of nonlinear systems using RBF neural networks," *IEEE Trans. Neural Netw.*, vol. 11, no. 1, pp. 69–79, Jan. 2000.

[38] Y.-K. Yang, T.-Y. Sun, C.-L. Huo, Y.-H. Yu, C.-C. Liu, and C.-H. Tsai, "A novel self-constructing radial basis function Neural-Fuzzy system," *Appl. Soft. Comput.*, vol. 13, no. 5, pp. 2390–2404, May 2013.

[39] M.-J. Lee and Y.-K. Choi, "An adaptive neurocontroller using RBFN for robot manipulators," *IEEE Trans. Ind. Electron.*, vol. 51, no. 3, pp. 711–717, Jun. 2004.

[40] F. F. M. El-Sousy, "Adaptive dynamic sliding-mode control system using recurrent RBFN for high-performance induction motor servo drive," *IEEE Trans. Ind. Informat.*, vol. 9, no. 4, pp. 1922–1936, Nov. 2013.

[41] J. Fei and T. Wang, "Adaptive Fuzzy-Neural-network based on RBFNN control for active power filter," *Int. J. Mach. Learn. Cybern.*, vol. 10, no. 5, pp. 1139–1150, May 2019.

[42] S. Hou, J. Fei, C. Chen, and Y. Chu, "Finite-time adaptive fuzzy-neural-network control of active power filter," *IEEE Trans. Power Electron.*, vol. 34, no. 10, pp. 10298–10313, Oct. 2019. doi: 10.1109/TPEL.2019.2893618.

[43] Y. Zhu and J. Fei, "Disturbance observer based fuzzy sliding mode control of PV grid connected inverter," *IEEE Access*, vol. 6, pp. 21202–21211, 2018.

[44] Y. Fang, J. Fei, and D. Cao, "Adaptive fuzzy-neural fractional-order current control of active power filter with finite-time sliding controller," *Int. J. Fuzzy Syst.*, vol. 21, no. 5, pp. 1533–1543, 2019. doi: 10.1007/s40815-019-00648-4.

[45] Z. Zhao, X. He, Z. Ren, and G. Wen, "Boundary adaptive robust control of a flexible riser system with input nonlinearities," *IEEE Trans. Syst., Man, Cybern., Syst.*, to be published. doi: 10.1109/TSMC.2018.2882734.

[46] Z. Zhao, J. Shi, X. Lan, X. Wang, and J. Yang, "Adaptive neural network control of a flexible string system with non-symmetric dead-zone and output constraint," *Neurocomputing*, vol. 283, pp. 1–8, Mar. 2018.

[47] Z. Zhao, Y. Liu, W. He, and F. Luo, "Adaptive boundary control of an axially moving belt system with high acceleration/deceleration," *IET Control Theory Appl.*, vol. 10, no. 11, pp. 1299–1306, Jul. 2016.

[48] Z. Zhao, X. Wang, C. Zhang, Z. Liu, and J. Yang, "Neural network based boundary control of a vibrating string system with input deadzone," *Neurocomputing*, vol. 275, pp. 1021–1027, Jan. 2018.

[49] S. J. Yoo, Y. H. Choi, and J. B. Park, "Generalized predictive control based on self-recurrent wavelet neural network for stable path tracking of mobile robots: Adaptive learning rates approach," *IEEE Trans. Circuits Syst. I, Reg. Papers*, vol. 53, no. 6, pp. 1381–1394, Jun. 2006.

[50] R.-J. Wai and C.-M. Liu, "Design of dynamic Petri recurrent fuzzy neural network and its application to path-tracking control of nonholonomic mobile robot," *IEEE Trans. Ind. Electron.*, vol. 56, no. 7, pp. 2667–2683, Jul. 2009.

[51] J. J. E. Slotine and W. Li, *Applied Nonlinear Control*. Upper Saddle River, NJ, USA: Prentice-Hall, 1991.

[52] K. J. Astrom and B. Wittenmark, *Adaptive Control*. New York, NY, USA: Addison-Wesley, 1995.

[53] O. Omidvar and D. L. Elliott, *Neural Systems for Control*. New York, NY, USA: Academic, 1997.

[54] L. X. Wang, *Adaptive Fuzzy Systems and Control: Design and Stability Analysis*. Englewood Cliffes, NJ, USA: Prentice-Hall, 1994.

[55] B. D. Anderson and J. B. Moore, *Optimal Control: Linear Quadratic Methods*. Englewood Cliffs, NJ, USA: Prentice-Hall, 1990.

[56] J.-S. R. Jang, C.-T. Sun, and E. Mizutani, *Neuro-Fuzzy and Soft Computing: A Computational Approach to Learning and Machine Intelligence*. Upper Saddle River, NJ, USA: Prentice-Hall, 1997.

[57] M. Krstic, I. Kanellakopoulos, and P. V. Kokotovic, *Nonlinear and Adaptive Control Design*. New York, NY, USA: Wiley, 1995.

FAYEZ F. M. EL-SOUSY (M'14) received the B.Sc. degree in electrical engineering from Menoufia University, Al Minufya, Egypt, in 1988, and the M.Sc. and Ph.D. degrees in electrical engineering from Cairo University, Giza, Egypt, in 1994 and 2000, respectively.

Since 1990, he has been with the Department of Power Electronics and Energy Conversion, Electronics Research Institute, Giza, Egypt, where he is currently a Full Professor. From August 1995 to June 2003, he was with the Department of Electrical Engineering, October Six University, Giza Egypt. From April 2004 to February 2007, he was a Postdoctoral Visiting Researcher with the Graduate School of Information Science and Electrical Engineering, Kyushu University, Fukuoka, Japan. From 2007 to 2010, he was with the Department of Electrical Engineering, College of Engineering, King Saud University, Riyadh, Saudi Arabia. From 2010 to 2014, he was with the Department of Electrical Engineering, College of Engineering, Salman Bin Abdulaziz University, Al-Kharj, Saudi Arabia. Since 2014, he has been with the Department of Electrical Engineering, College of Engineering, Prince Sattam bin Abdulaziz University, Saudi Arabia. His research interests include modeling and control of motor drives, motion-control systems, wind energy systems, digital signal processing-based computer control systems, computational intelligent of power electronics and electric drives, intelligent control theories including fuzzy logic, neural networks, and wavelets, nonlinear control and optimal control, and robust control, especially in the intelligent control of Maglev vehicle transportation systems.

MOHAMED F. EL-NAGGAR received the B.Sc., M.Sc., and Ph.D. degrees from Helwan University, Egypt, in 1995, 2002, and 2009, respectively, all in electrical engineering, where he was with the Department of Electrical Power and Machines Engineering, Faculty of Engineering, from 1995 to 2013. Since 2013, he has been an Assistant Professor with the Department of Electrical Engineering, College of Engineering, Prince Sattam Bin Abdulaziz University, Saudi Arabia. His main research interests include power system protection and switchgears, power transformers operation, testing, and maintenance.

MAHMOUD AMIN (S'09–M'12–SM'16) received the B.Sc. and M.Sc. degrees in electrical engineering from Helwan University, Egypt, in 2003 and 2008, respectively, and the Ph.D. degree from Florida International University, Miami, FL, USA, in 2012. Since 2012, he has been an Assistant Professor with the Manhattan College, Riverdale, NY, USA, and Researcher with the Electronics Research Institute. Since 2018, he was promoted to an Associate Professor with Manhattan College. He has published more than 40 articles in professional journals and conference proceedings. His current research interests include power electronics in sustainable energy systems, adjustable speed drives, and smart grid security. He was a recipient of the GSA Scholarly Forum Prize Paper Award 2010 and the IEEE PES GM 2010 Contest Award. He is Editor of the IEEE TRANSACTIOSN ON ENERGY CONVERSION and the IEEE TRANSACIONS ON MAGNETICS.

AHMED ABU-SIADA (M'07–SM'12) received the B.Sc. and M.Sc. degrees from Ain Shams University, Cairo, Egypt, in 1998, and the Ph.D. degree from Curtin University, Bentley, WA, Australia, in 2004, all in electrical engineering, where he is currently an Associate Professor with the Department of Electrical and Computer Engineering. His current research interests include power system stability, condition monitoring, power electronics, and power quality. He is the Vice-Chair of the IEEE Computation Intelligence Society, WA Chapter. He is the Editor-in-Chief of the *International Journal Electrical and Electronic Engineering*. He is a Regular Reviewer for various IEEE Transactions.

KHALED A. ABUHASEL received the B.Sc. and M.Sc. degrees from the University of Central Florida, Orlando, FL, USA, in 2009 and 2010, respectively, and the Ph.D. degree from New Mexico State University, Las Cruces, NM, USA, in 2012, all in industrial engineering.

He is currently an Associate Professor with the Mechanical Engineering Department, University of Bisha, Saudi Arabia. He holds three U.S. patents, and more than 35 publications in journals and proceeding of very reputable conferences. His research interests include optimization, systems engineering, health care systems, intelligent systems, artificial neural network methodologies, and statistical analysis.